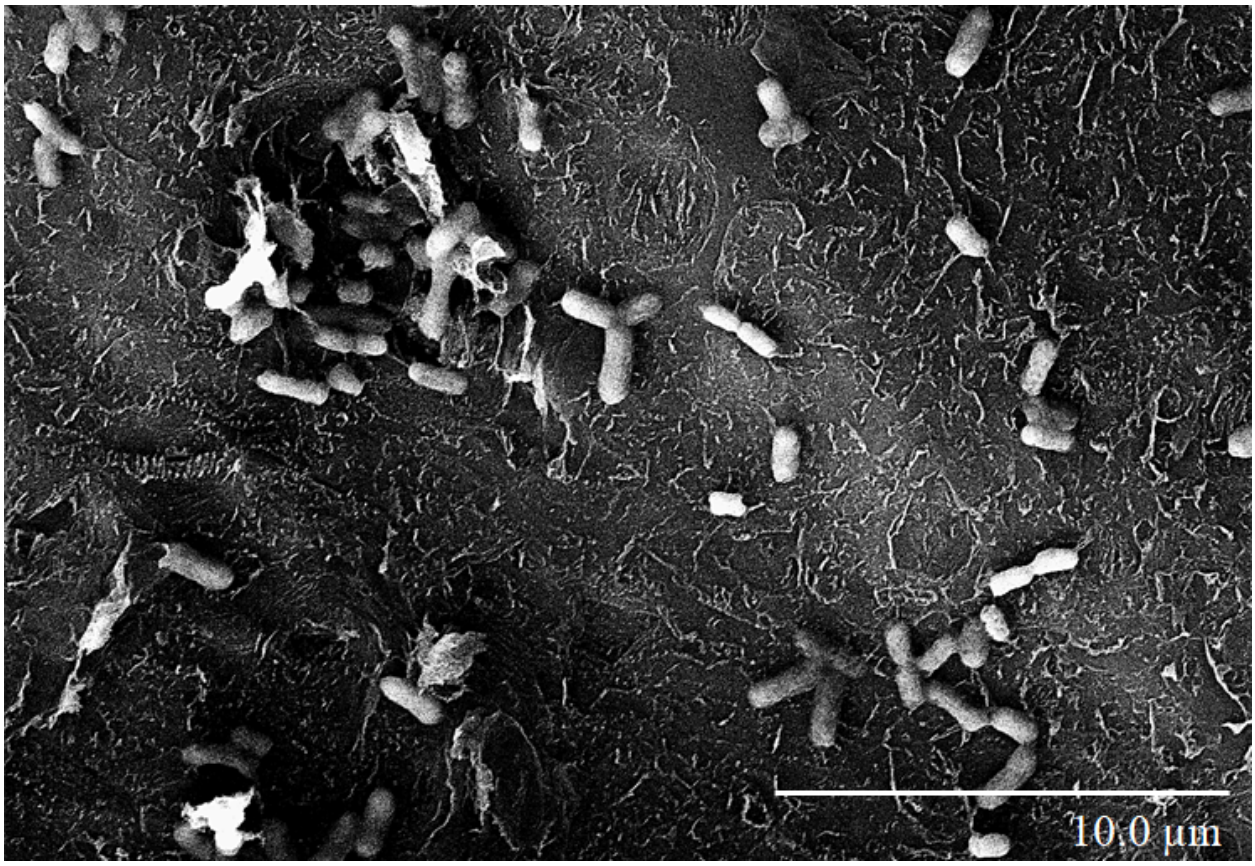

Chalmers University of Technology

Deposition of Graphene-Based Nanoflakes on Polymer Substrates for Scalable Production of Antibacterial Medical Devices

Master's thesis in Materials Chemistry

PETRA AL-YOUSIFI

DEPARTMENT OF CHEMISTRY AND CHEMICAL ENGINEERING
CHALMERS UNIVERSITY OF TECHNOLOGY
Gothenburg, Sweden 2026
www.chalmers.se

Master's thesis 2026

Uniform Deposition of Graphene-Based Nanoflakes on Polymer Substrates for Scalable Production of Antibacterial Medical Devices

Petra Al-Yousifi

CHALMERS
UNIVERSITY OF TECHNOLOGY

Department of Chemistry and Chemical Engineering
Chalmers University of Technology
Gothenburg, Sweden 2026

Uniform Deposition of Graphene-Based Nanoflakes on Polymer Substrates for Scalable Production of Antibacterial Medical Devices
PETRA AL-YOUSIFI

Supervisor: Martin Lovmar, Wellspect
Examiner: Martin Andersson, Department of Chemistry and Chemical Engineering

Master's Thesis 2026
Department of Chemistry and Chemical Engineering

Chalmers University of Technology
SE-412 96 Gothenburg
Telephone +46 31 772 1000

Cover: Image of bacteria on a lasered graphene-oxide nanoflakes coating captured by a scanning electron microscope.

Typeset in LaTeX
Printed by Chalmers Reproservice
Gothenburg, Sweden 2026

Uniform Deposition of Graphene-Based Nanoflakes on Polymer Substrates for Scalable Production of Antibacterial Medical Devices
PETRA AL-YOUSIFI
Department of Chemistry and Chemical Engineering
Chalmers University of Technology

Abstract

Catheter-associated urinary tract infections are a worldwide problem that is usually solved with antibiotics, leading to an increased risk of antibiotic resistance which is a global threat. A way of decreasing the prescription of antibiotics is reducing the risk of infections by mechanically killing the bacteria or inhibiting its ability to attach and create a biofilm on the surface of a catheter. This may be achieved with sharp vertically aligned graphene-based nanoflakes on the polymeric surface. The aim of the study was to identify a robust and effective method for a homogeneous deposition of graphene-based nanoflakes onto a polymeric surface for scalable production. To explore materials and methods a screening process was done before creating the final samples. The samples were made using plasma and flame treatments in combination with drop casting and dip coating methods. Surface characterization of the samples was performed with scanning electron microscopy and atomic force microscopy. The results showed that a homogeneous coating in combination with laser treatment can achieve vertically aligned nanoflakes structure with different densities depending on the amount of deposited graphene-based nanoflakes.

Keywords: Graphene, graphene oxide, nanoflakes, nanomaterials, dip coating, drop casting, antibacterial effect, catheters, thermo-plastic elastomer.

Acknowledgements

I would first and foremost like to express my gratitude towards my supervisor Professor Martin Lovmar for the continous support, interesting discussions and guidance during the project. I also want to thank Wellspect, Dentsply Sirona, for providing the resources to make this thesis possible, and the colleagues there who have been very helpful and provided assistance whenever I had questions or needed access to various instruments. This work was carried out within the framework of the SIO Graphene strategic innovation program, a joint initiative funded by Vinnova, Formas, and the Swedish Energy Agency. I want to thank them for making this work possible.

I am grateful to Docent Santosh Pandit, for performing the antibacterial testing of my samples at Chalmers, the excellent collaboration and continues support during the project. I would also like to thank Associate Professor Magnus Engholm, for conducting the laser treatment of my samples at the Mid University and a great collaboration.

I want to thank Professor Martin Andersson for always answering questions, giving support and valuable advice throughout the thesis and enabling the use of atomic force microscopy at Chalmers.

I also want to thank family and friends for support during the project. Last, but not least, I want to thank Chalmers University of Technology for five years of exceptional education and experiences.

Petra Al-Yousifi, Gothenburg, June 2026

List of Abbreviations

List of Abbreviations

Below is the list of abbreviations that have been used throughout this thesis listed in alphabetical order:

AFM	Atomic Force Microscopy
BSE	Backscattered Electrons
CAUTI	Catheter-Associated Urinary Tract Infection
E. coli	*Escherichia coli*
GNFs	Graphene-based Nanoflakes
GNMs	Graphene-based Nanomaterials
GO	Graphene Oxide
HAIs	Healthcare-Associated Infections
PE	Primary Electrons
rGO	reduced Graphene Oxide
S. aureus	*Staphylococcus aureus*
SE	Secondary Electrons
SEM	Scanning Electron Microscopy
TPE	Thermoplastic Elastomer
UTIs	Urinary Tract Infections

Contents

List of Figures

List of Tables

1
Introduction

Healthcare-associated infections (HAIs) are a worldwide problem and cost about €7 billion every year for the European healthcare systems [1]. The majority of HAIs are urinary tract infections (UTIs) and bloodstream infections which are caused by medical invasive devices such as urinary and central venous catheters [2]. Urinary and central venous catheters create a platform for biofilms to develop on the surface, leading to infections that are treated with antibiotics which increases the risk of the development of antibiotic resistance. Antibiotic resistance is a threat to global health as it results in longer hospital stays and increases mortality rates [3]. A "SIO-grafen"-funded project was therefore initiated with the objective to develop a safe and effective medical device with a graphene-based surface with antibacterial properties. The antibacterial property is based on the 2D-structure of graphene that could be attached to the surface of the device to mechanically prevent biofilm formation. It has previously been demonstrated that laser treatment of a graphene coated polymer surface has the potential to create a surface with antimicrobial effect, but further development of the process is required to make it robust and scalable.

1.1 Background

1.1.1 Catheter Associated Urinary Tract Infections

Catheterassociated urinary tract infections (CAUTIs) are infections that occur in the bladder caused by the use of catheters. For an infection to be classified as a CAUTI, the infection must occur 48 hours or more after the catheter has been inserted [4]. The majority of the infections are caused by indwelling catheters, and the risk for infections increases with the catheterization time [5][4]. UTIs can be caused by gram-positive and gram-negative bacteria. Two common bacteria causing UTIs are *Escherichia coli* (*E. coli*) causing up to 75% of UTIs and *Staphylococcus aureus* (*S. aureus*) causing up to 3% of UTIs [6]. *E.coli* is a gram-negative bacteria, that is characterized by its rod-shaped structure [6][4]. *S.aureus* is a gram-positive bacteria and is characterized by its spherical shape [7].The main difference between

gram-positive and gram-negative bacteria is the structure of their cell wall. Gram-positive bacteria have a relatively thick layer of peptidoglycan which is the main structural component of the cell wall. The peptidoglycan layer provides mechanical strength, and is located on the outer part of the cell wall of gram-positive bacteria [8]. Gram-negative bacteria have a relatively thin layer of peptidoglycan surrounded by both an outer and inner membrane [9]. Antibiotics are drugs used to treat infections caused by harmful gram-positive and gram-negative bacteria by inhibiting the bacterial growth without causing harm to the host [10][11]. Antibiotic resistance occurs by misuse and overuse of antibiotic drugs, where a bacterial group that survives antibiotic treatment gradually starts dominating by natural selection [11]. Antibiotic resistance is a global threat and if left unsolved, will lead to an estimated annual death of 2 million people by 2050[12]. Therefore, other alternatives for fighting infections need to be studied. One strategy to counteract the risk of antibiotic resistance is by mechanically killing the bacteria or inhibiting their ability to attach to the surface of a medical device and forming biofilms. The sharp structure of graphene-based nanoflakes (GNFs) is one approach to solving this problem.

1.1.2 Antimicrobial Effect of Graphene-Based Nanoflakes

The antimicrobial effect of GNFs has been widely studied in the previous years, making it interesting for the biomedical field. It has been shown with different microbiology testing methods that GNFs can kill bacteria and prevent bacterial attachment on different surfaces [13][14][15]. Some studies suggest that cell death is caused by oxidative stress caused by reactive oxidative species (ROS). ROS are proposed to be induced by GNFs that wrap around the bacterial cell [14]. However, for wrapping to occur, the lateral size of the GNFs would need to be micrometer sized, and in previous studies, GNFs coatings with horizontal alignment on the surface showed no antibacterial effect. Therefore oxidative stress caused by wrapping can be ruled out in this study [13][16]. Another proposed reason for the antibacterial effect of GNFs is the sharp edges of vertically aligned GNFs on a surface. When bacteria interacts with the surface, the sharp edges pierce the cell wall which damages the bacteria and gives an antifouling-effect [15][13]. While bacterial cell death could reduce the risk for infections, it may also lead to loss of antifouling effect due to dead bacteria stacking up and creating a flat "dead biofilm" on the surface. Therefore, the antifouling-effect of the sharp edges of vertically aligned GNFs, would likely have a better long-term effect for prevention of bacterial-adhesion to the surface.

Previous studies did antimicrobial testing on graphene nanomaterials (GNMs) that were integrated in agar plates [17]and coated on metal and SiO_2 surfaces [13]. In complementary studies, GNMs were incorporated into a polymer matrix as a composite material where graphite nanoplatelets were aligned through extrusion in the polymer matrix and etched to expose the platelets on the surface [18]. These studies showed that the antibacterial effect is dependent on two parameters; the density and orientation of the GNFs on the surface. The GNFs need to be perpendicular to the surface as it has been shown that horizontally aligned GNFs have no antibacterial properties [13]. The GNFs sharp edges induce membrane stress [16] and makes bac-

terial attachment to the surface difficult. In one study, laser was utilized to induce graphene formation on polyimide sheets creating a hydrophobic surface [19]. In this project, laser is used to create vertically aligned GNFs coatings on polymeric material used for urinary catheters. For the laser treatment to work, it is important that the thickness of the GNFs coating is homogeneous. To achieve a homogeneous thickness of GNFs on the surface, the methods utilized for the deposition need to be effective, scalable and standardized.

1.1.3 Methods for Deposition of GNFs

There are different ways to coat a surface with GNFs. In previous studies, chemical vapor deposition (CVD) was utilized, which is a bottom-up method to synthesize GNFs on large areas [20]. Precursors in gas phase react and deposit onto a substrate surface and it is difficult to control the orientation of the nanoflakes. Therefore, plasma-enhanced chemical vapor deposition (PECVD) can be used for vertical deposition of graphene nanoflakes [13]. CVD and PECVD is done in relatively high temperatures, making it unsuitable for polymer surfaces.

Another potential method for homogeneous deposition of GNFs is spray coating. Spray coating has been used in various applications, some of them being coating of medical devices for drug-delivery, increased osseointegration and anti-fouling properties [21]. One spray-coating technique used for coating of medical devices is the ultrasonic spray nozzle where atomization of the coating solution into a fine spray is done using high frequency sound vibrations [21][22]. Spray coating the surface with multiple layers to achieve a desired thickness have shown results of a homogeneous thickness of GNMs coatings across polymeric substrates [22][23]. However, in this project, the GNFs dispersions have very low viscosity. When spraying thin liquid on a hydrophobic surface droplets will be formed, giving a similar effect to drop casting.

Drop casting is a simple method used to coat small surfaces by dropping a dispersion of particles on the surface and letting the solvent evaporate, leaving the dilute on the surface [24] as seen in Figure 1.1.

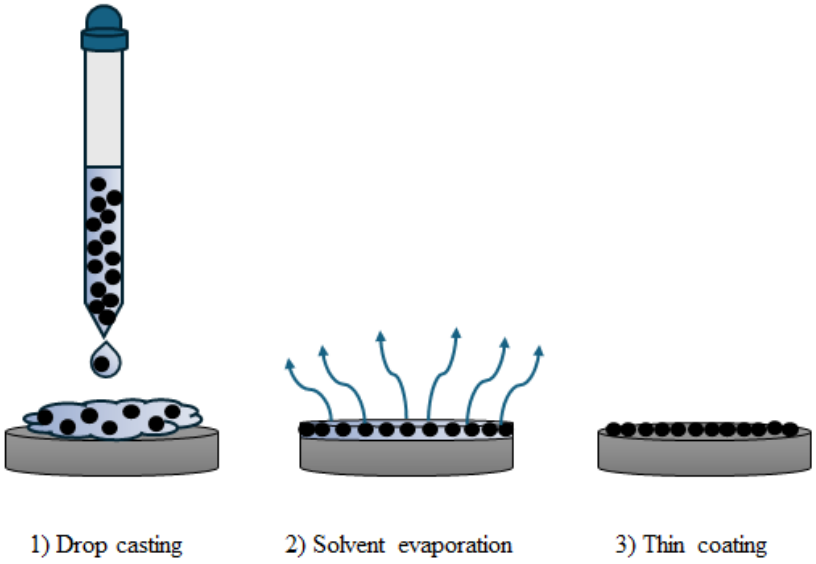

Figure 1.1: Illustration of the drop casting method. The first step includes dropping the dispersion onto the substrate. In the second step the solvent evaporates leaving a thin coating of dilute on the surface.

Drop casting can be combined with spin coating to get a thin homogeneous coating [23]. However spin coating is hard to scale up, especially for non-flat surfaces. Dip coating, is another simple method, where the substrate is dipped in the dispersion and withdrawn, leaving a layer of wet film on the surface where the solvent eventually evaporates and the dilute is left on the surface [23] as shown in Figure 1.2.

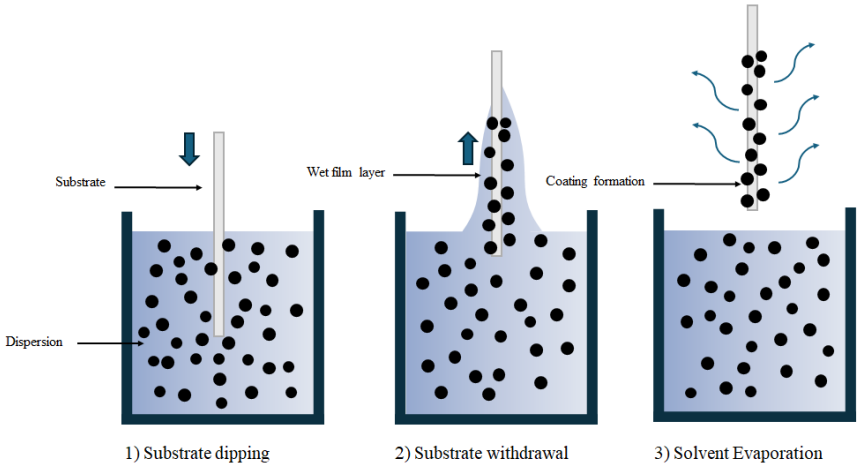

Figure 1.2: Illustration of the dip coating method including dipping of the substrate, withdrawal of the substrate and solvent evaporation leaving a coating of dilute on the surface.

For both dip coating and drop casting, it is important that the wettability of the surface is high for better distribution of the dilute across the surface. Dip coating is an effective method for scale up.

1.2 Aim

The aim of the thesis project was to identify simple robust methods for applying GNFs homogeneously onto a polymer surface in a scalable way and create standard methods for the deposition, making standardization of the laser treatment possible.

1.3 Limitations

The thesis project did not involve the production of the polymer substrates or GNFs, but was provided by Wellspect. The laser treatment of the GNFs coated substrates was conducted by partners from Mid-Sweden University and the microbiological testing of the laser treated substrates was conducted by partners at Chalmers. In previous studies, the antimicrobial effect was analyzed with scanning electron microscopy in combination with colony-forming unit (CFU) count, which gave a qualitative and quantitative result of the reduction in biofilm formation in comparison to a control surface. CFU count could not be performed in this study due to the time limit and not enough control area. The plasma machine which was used before the drop casting method broke during the thesis and could not be repaired before the end of the project and therefore could not be used for the rest of the project including the pilot-process. The pilot-process was conducted with an employee from Wellspect who needed to monitor the whole process closely and needed to prepare the pilot plant. The preparation and process were time-consuming and was conducted twice near the end of the project. This meant that the use of flame treatment was limited and could only be done before the pilot-process and once for contact angle measurement. Atomic force microscopy could only be done on one of the samples that were sent for laser treatment as there was not enough time to send them back, and therefore was done on a surface with similar structure from a previous study.

2

Theory

2.1 Graphene-based Nanomaterials Structure and Applications

2.1.1 Graphene, Graphene Oxide and reduced Graphene Oxide

Graphene has gained a lot of attention the last two decades and is a modern carbon-based material with unique properties due to its 2D-structure with a thickness of one atomic layer and a hexagonal arrangement of carbon atoms [25] [19] [26]. Graphene has an estimated thickness of 0.345nm [27]. It is made from graphite which simply consists of many graphene sheets stacked onto each other making a 3D-material and is a naturally occuring allotrop. One-layer graphite is called graphene, two and three layer graphene is called bi- and trilayer graphene, and less then 10 layers is called few-layered graphene [28]. Graphene oxide (GO) is an oxidized form of graphene and a lot of oxygen-containing functional groups are present in its structure, such as carboxyl groups, hydroxyl groups as well as epoxy groups which makes it hydrophilic and very dispersible in polar solvents such as water [29]. Reduced graphene oxide (rGO) is the reduced version of GO and is less hydrophilic due to fewer oxygen-containing functional groups in its structure[28] as illustrated in Figure 2.1

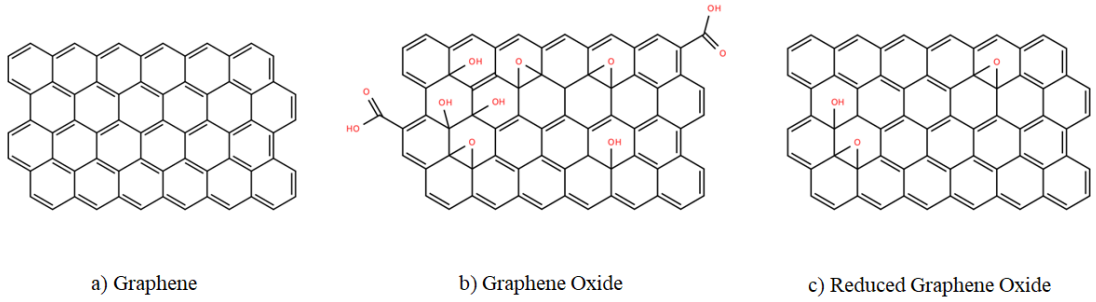

Figure 2.1: Chemical structure of three different GNFs a) Graphene, b) Graphene oxide, c) reduced graphene oxide

The hexagonal structure gives the material great strength, conductivity and other properties thanks to the sp^2-hybridized carbon atoms with alternating double and single bonds. The synthesis of GNMs is well established and can be performed either by a bottom-up or top-down method [30].

2.1.2 Graphene-Based Nanoflakes

GNFs are fragments of graphene-based sheets and are finite in both dimensions with thickness in the nanometer regime and lateral size in the micrometer regime giving it a high aspect ratio[31][32]. GNFs can be made from top-down method starting from graphite, by separating each graphene-based layer through common methods like ultrasonic and liquid-phase exfoliation to produce GNFs water dispersions [33]. A bottom-up method is CVD. GFNs have a wide potential in the materials science field and can be used in energy systems, composite materials and for surface coatings. An intrinsic property of graphene-based sheets is that they have ripples making them naturally wrinkly due to out-of-plane deformations[34].

2.2 Surface Properties and Wettability of Polymer Surfaces

2.2.1 Surface Free Energy

An important property affecting the interaction between a polymer solid surface and a liquid is the surface free energy. Surface energy can be defined as the energy

required to create a unit surface area [35] and is measured in $J/m^2 = N/m$. The surface atoms of the material do not have neighboring atoms that fill their outer orbitals like the bulk atoms, leading to dangling bonds [36]. Dangling bonds at the surface increase the surface energy and nature always strives to reduce the free energy which can be done by interacting with foreign molecules. Increased surface energy leads to increased adhesion [37][35].

2.2.2 Surface Roughness

All solid surfaces have irregularities or deviations from their intended geometrical form on micro- and nanoscale [38][39]. These irregularities can be referred to as roughness of a surface and can occur due to the processing-parameters of the material [40]. The surface roughness of a material increases the surface area which increases the density of dangling bonds. An increase in dangling bonds increases the surface energy [36]. If a surface initially is hydrophobic, the surface will be more hydrophobic if the roughness is increased, and vice versa for a hydrophilic surface. This phenomena is called super hydrophobicity and super hydrophilicity [41][42]. Fabrication of super hydrophobic and hydrophilic surfaces can be achieved by plasma or UV treatment of a surface [42]. While the surface area is increased, it also creates gaps where hydrophobic gases such as air can get trapped, giving a hydrophobic effect [42]. Surface roughness can have an impact on physical properties of a material such as adhesion to the surface or surface wettability [43].

2.2.3 Wetting of Polymer Surfaces

Wetting is defined as the ability of a liquid to spread on a surface [44][45]. The spreading depends on three different forces acting on the liquid, surface free energy of the solid (γ_{SG}), interfacial tension between the solid and liquid (γ_{SL}) and the surface tension of the liquid (γ_{LG}) according to Young´s equation 2.1

$$\gamma_{SG} = \gamma_{SL} + \gamma_{LG} \cos\theta_c \tag{2.1}$$

where $\cos\theta_c$ is the contact angle between the solid and the liquid and is directly affected of the balance between the interfacial forces [44][45]. The surface tension arises from the asymmetry of the attracting forces between the molecules in the bulk of the liquid compared to the molecules at the surface. In the bulk of the liquid, the molecules sense the same attracting forces in all directions, whereas the molecules at the surface are not balanced in one direction [44]. The liquid therefore tries to minimize its surface to lower the free energy by changing its shape so it achieves the minimum surface area keeping a constant volume [46]. Higher surface free energy leads to better wetting, as the surface strives to interact with the liquid to reduce its energy. Solid polymeric materials contain long hydrophobic carbon chains and usually have very low surface free energy, leading to poor wetting [47] as shown in Figure 2.2.

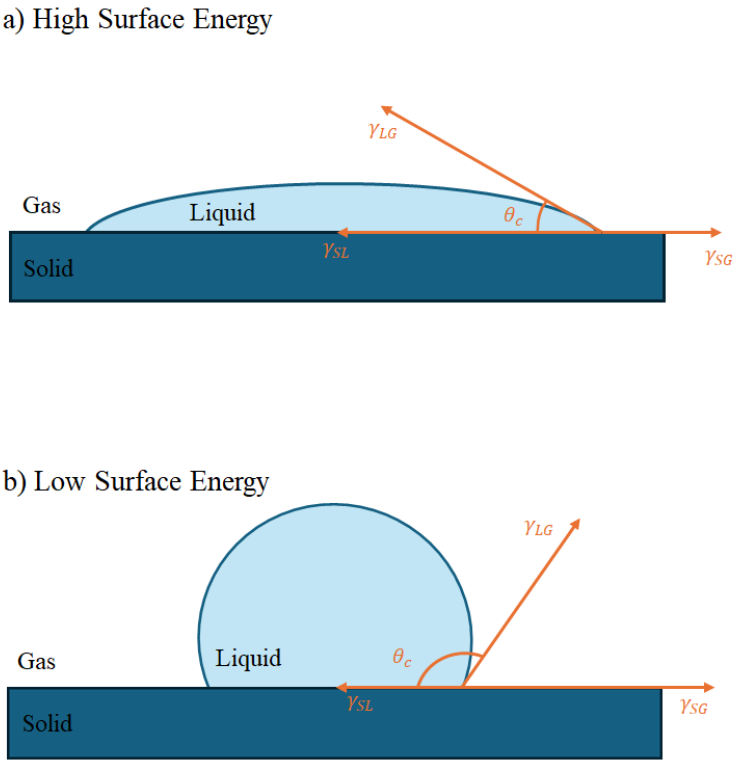

Figure 2.2: Surface forces acting on a liquid spreading on a solid surface with a) high surface energy and b) low surface energy.

When the intermolecular forces of a liquid are stronger than the attracting forces of the surface, droplets with high contact angle forms to reduce their surface area, hence its contact with the solid surface. Wetting of a polymer with a solvent can be increased by choosing a solvent with low surface tension, adding a surfactant to reduce the interfacial tension between the solid and the liquid or increasing surface energy of the solid [44]. Increasing the surface energy of a polymer can be done by for example adding a hydrophilic additive to the polymer matrix, plasma treatment that introduces hydrophilic functional groups to the surface or by flame treatment[11][48].

2.3 Water-Ethanol Mixtures

The most important and common green solvent in the world is water, also called the universal solvent [49][50][51]. Ethanol is a commonly used green solvent [52][51][53] and has a hydroxyl-group that is hydrophilic and makes it miscible in solvents like water due to hydrogen-bonding. Ethanol also has a hydrophobic ethyl group linked to the hydroxyl-group [51].The hydrophobic and hydrophilic parts of the ethanol molecule gives it amphiphilic attributes [54]. As seen in Table 2.1, water has a relatively high surface tension compared to ethanol.

Table 2.1: Viscosity and surface tension of water and ethanol at 20 °C [45][55].

Substance	Viscosity (mPa · s)	Surface tension (mN/m)	Vapor Pressure (kPa)
Water	1.00	72.8	2.34
Ethanol	1.07	22.4	5.95

Ethanol has very low surface tension, low viscosity and high volatility. Water has almost the same viscosity as ethanol, but more than three times higher surface tension and less then half as volatile. This is due to the strong hydrogen bonding between the water molecules within the bulk. In theory, this would make a water and ethanol mixture have almost the same viscosity, but lower surface tension and higher volatility than a 100 wt% water solution. The use of water and ethanol as solvents for industrial processes is in accordance with the green principles, 5, 6, 7 and 12 [56].

2.4 Surface Treatments

2.4.1 Plasma Treatment of Polymer Surfaces

Plasma treatment can be used for various purposes such as surface cleaning, elimination of organic compounds, etching, patterning and increasing surface energy [36][37][48]. Plasma can be generated by gases such as air, N_2 and O_2 gas that enter the vacuum chamber where a microwave field is applied. Plasma generated by air has a purple/pink color as illustrated in Figure 2.3.

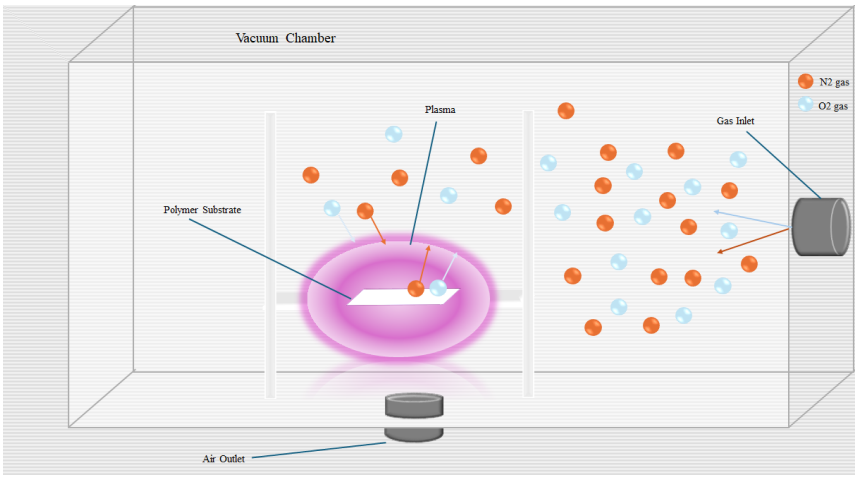

Figure 2.3: Illustration of a vacuum chamber with plasma generated by an airflow and a microwave field.

The microwave field accelerate free electrons that collide with gas molecules which causes the gas to ionize, dissociate and generate plasma containing electrons, radicals excited atoms and UV photons [48]. The radicals and ions accelerate towards the surface and can cause adsorption and desorption of radicals, abstraction of hydrogen from the surface and ions that knock out parts of the surface changing the surface topography [37][48].

2.4.2 Flame Treatment of Polymer Surfaces

Flame treatment is a commercial surface preparation technique where the surface is exposed to a flame for a short period [57][58]. It is a process that is used to increase the surface energy of polymeric materials [58]. The material is moved across a fixed flame that is oxidizing and and contains excited fragments of oxygen containing functional groups and atomic oxygen that abstract hydrogen from the surface and replaces them with functional groups such as carbonyl, carboxyl and amide functional groups [57][58]. This increases the surface wettability and adhesion of the polymeric materials. Only 4–6 nm of the surface depth is affected by this treatment [57].

2.5 Thermoplastic Elastomers Interaction with GNFs

Thermoplastic elastomers (TPE) are polymeric materials that consist of a physical blend of plastic and elastic polymers, giving them both rubber-like and thermoplastic properties [59][60]. Polymeric surfaces mostly contain long hydrophobic carbon chains, whereas GO is hydrophilic and contains polar functional groups. The interaction between a polymeric surface and GO is therefore mainly limited to van der Waals forces. However, plasma or flame treatment can introduce polar groups onto the polymer surface [48][58]. Once these polar groups are present, GO nanoflakes can form hydrogen bonds and stronger interfacial interactions with the surface, improving adhesion at the interface.

2.6 Analytical Methods

2.6.1 Profilometer

To measure the roughness of a surface, a profilometer can be used. A stylus with a pointy tip moves across the x-axis of a surface and measures differences in the z-axis as shown in Figure 2.4. The small tip of the stylus that has a radius of about $20\mu m$, is the only thing in contact with the sample. The needle is connected to a measuring instrument that detects the differences in the y-axis as a signal that is sent to a computer and gives a surface roughness profile and different roughness parameters.

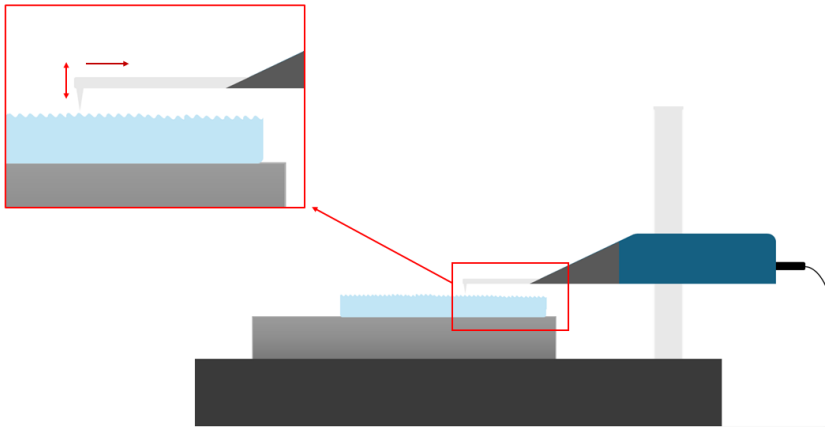

Figure 2.4: Illustration of a profilometer and its stylus in contact with the substrate surface.

Ra, Rdc, RSm and RPc are four roughness values that can be measured with a profilometer. The Ra value of a surface is defined as the arithmetic average roughness, an average value of the lowest and highest points in the z-axis of the roughness profile [61][62]. A smooth surface has a low Ra value and a rough surface like sandpaper has a high Ra value. Rdc is a measurement of the depth of a materials surface between two statistically defined levels and describes the depth of the main roughness structure or the "valleys" of the surface [61][62]. The density of the valleys or bumps on the surface can be described by a RSm value which is defined as the mean spacing of the irregularities [62][61]. RPc is defined as the peak count of the surface and measures the amount of bumps and peaks per unit length [62][61].

2.6.2 Contact Angle Measurement

The sessile-drop method is a experimental technique for measuring the contact angle between a liquid droplet and a solid surface. The setup contains a flat substrate surface, a liquid that is pushed out of a needle and a camera that live captures images and measures the contact angle by an ellipse-fitted tangent to the three phase point [63] as illustrated in Figure 2.5.

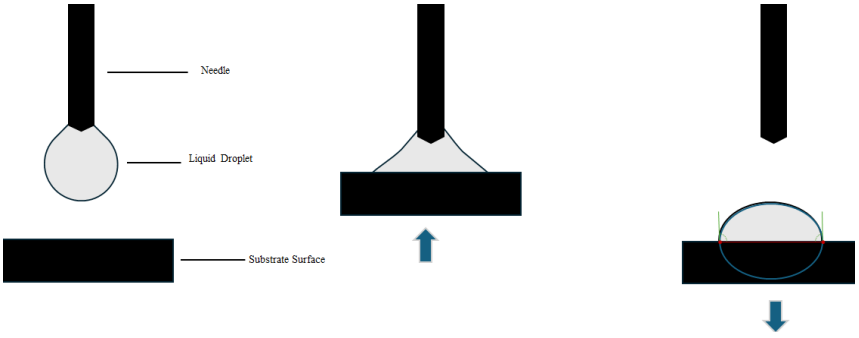

Figure 2.5: Contact angle measurement using sessile-drop method.

2.6.3 Scanning Electron Microscopy

Scanning Electron Microscopy (SEM) is an analytical instrument used to analyze surface topography and morphology by bombarding the specimen with primary electrons (PE) using a focused electron beam, where back scattered electrons (BSE) and secondary electrons (SE) can be detected as illustrated in Figure 2.6.

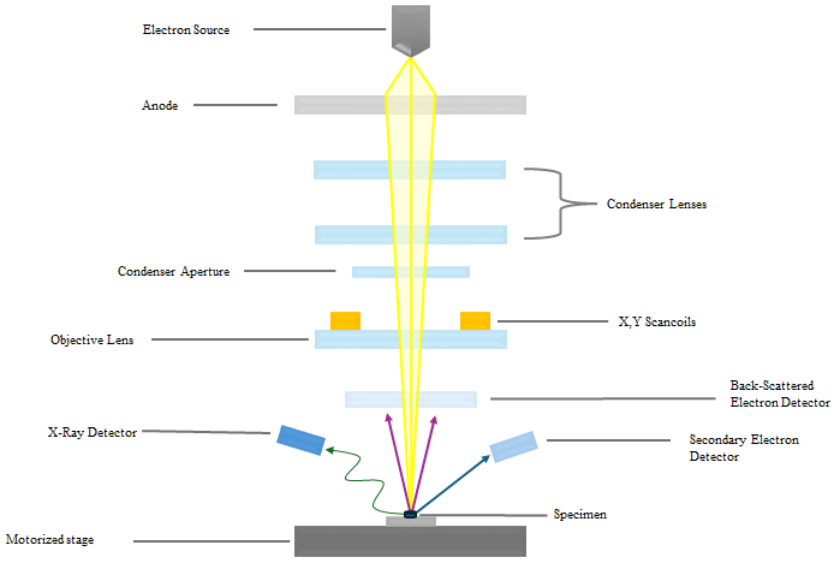

Figure 2.6: Working principle of SEM.

BSE are PE that have been elastically scattered, are high in energy and give compositional contrast. When high energy PE interact with the specimen, some of the energy can be transferred and knock out electrons from the specimen atoms, which are low in energy and called SE. SE are inelastically scattered and give topographical information. Specimen preparation includes removing all solvent and moisture, mounting it firmly and ensuring the surface conductivity of the specimen to avoid charge build up [64][65][66].

2.6.4 Atomic Force Microscopy

Atomic force microscopy is an analytical instrument that gives high-resolution nanometer spatial 3D-images of surfaces [67]. The AFM components consists of a cantilever with a sharp probe, less then a 50 nm radius [68] that raster scans the sample surface, a piezoelectric scanner achieving nano-positioning on the XYZ directions and a laser beam directed at the cantilever that is reflected and detected by a photodiode [67][69]. The working principle of AFM is based on the interactive forces between the tip of the probe and sample surface causing the cantilever to bend when it senses irregularities and deflect the laser which is processed into a signal [67][69]. There are different operating modes which can be utilized depending on the sample sensitivity.

Contact mode is when the probe tip is in constant contact with the surface of the sample and is deflected when in contact with the surface peaks or valleys [69][67].

The tip of the probe is to maintain a constant deflection and is constantly adjusted to keep the same height above the surface. Non-contact mode is when the tip of the probe is not in contact with the surface but about 5–20 nm far away from the sample [69]. In non-contact mode the tip oscillates near the surface and the changes to the resonant frequency or amplitude of the cantilever that occur due to Van der Waals and electrostatic forces are detected [69] [67]. Tapping mode, also called intermittent mode is when the tip of the probe both intermittently taps and oscillates near the surface. Tapping mode is preferred over contact mode for sensitive samples as it exerts less lateral force on the sample compared to contact mode. However, contact mode is preferred if the sample tolerates the force without deforming as it scans across the surface faster and gives higher resolution [69].

3
Method

3.1 Materials

3.1.1 Polymer Substrates

Four different kinds of TPE materials were provided by Wellspect, which in this thesis will be referred to as Julien 1-4. The substrates came in the shape of rectangular plates with a rough side and a smooth side and tubes representing the catheter shape. Julien 1 is almost the same as the catheter material used in present production. Three of the TPE substrates, Julien 2-4 have a hydrophilic additive in their polymer matrix for the purpose of increasing the surface energy and wetting of the surface as seen in Table 3.1.

Table 3.1: TPE materials with and without hydrophilic additives.

Material	**Hydrophilic additive**
Julien 1	No additive
Julien 2	Additive X
Julien 3	Additive Y
Julien 4	Additive Y + modified TPE matrix

Both additives are bio-based and used to lower the surface tension between polymer surface and water. Additive X is a low-viscosity liquid that blends into the TPE and is usually used as an emulsifying agent, typically forming water-in-oil emulsions. Additive X has a ring-shaped backbone together with hydrophobic chains and a number of polar functional groups, giving it amphiphilic character. Additive Y is a paste-like additive and has a linear hydrophobic backbone with accessible polar groups and usually keeps oil suspended in water. The additives are not crosslinked to the polymer and can migrate through the material and therefore to the surface, making it more hydrophilic.

3.1.2 GNFs Dispersions

A GNFs water dispersion was purchased with a GO concentration of 4 mg/ml and is hereafter referred to as dispersion A. 90% of the GNFs have a lateral size of <5-7 μm, 50% have a lateral size of <2-4 μm and 10% <1-2 μm as shown in Table 3.2.

Table 3.2: Purchased GNFs water dispersion.

Dispersion	GO (mg/ml)	Lateral Size (μm)	D90	D50	D10
A	4		5–7	2–4	1–2

GNFs tend to aggregate due to $\pi - \pi$ stacking, hydrogen bonding and van der Waals forces [70], therfore the purchased GNFs water dispersions were first sonicated using a Elmasonic S 60H ultrasonic bath for 30 minutes and then diluted into two different GNF concentrations and sonicated again for 30-60 minutes.

3.1.3 Dilution of GNFs Dispersions

Dispersion A was diluted with 99.7% absolute ethanol according to table 3.3

Table 3.3: Diluted dispersions concentration of GNFs and water/ethanol (wt%).

Diluted Dispersion	GO (mg/ml)	Water/Ethanol (wt%)
A1	1	30/70
A2	2	56/44

into dispersion A1 and dispersion A2.

3.2 Screening Process

The screening process consisted of a comparative analysis between the different materials (Julien 1-4) and the different shapes (plates and tubes) to find out which material of the four is the optimal for a scale up process and if the conclusions drawn from the experiments and analysis done on the plates could be applied on the tubes. This was done by analyzing the surface roughness, surface wetting by contact angle measurements, SEM analysis to compare topography and surface structure and exploring different GNFs dispersions by the drop casting method on the surfaces.

3.2.1 Roughness Measurements of the TPE Plates Rough and Smooth Side

To identify the side of the plates on which the drop casting was performed, the surface roughness of each side was evaluated and compared to the tubes of Julien 1-4. For each TPE material, the roughness values of the smooth and rough sides were

measured using a Hommel Wave Waveline 20 profilometer. A piece of each TPE material was cut out and placed under the probe. Three measurements were done on each substrate and the mean value of the three measurements was calculated by the software of the instrument. The mean roughness of each side was then compared to the mean roughness of the tube samples.

3.2.2 Contact Angle Measurement

Contact angles were determined using the sessile drop method with a DSA 100 drop shape analyzer instrument. The contact angle measurement was done to evaluate the wetting of each TPE surface with the different diluted dispersions and the effect of plasma and flame treatment. The liquid medium used in the needle did not contain any GNFs due to risk for accumulation of GO inside the needle causing clogging or contamination. However, different wt% of water and ethanol was tested. The liquid medium was prepared using Milli-Q water and 99.7% absolute ethanol. The wt% ratio of water and ethanol that gave a low contact angle while still allowing for a reasonable concentration of GNFs was later used to continue with the experiments.

3.2.3 Plasma Treatment of the Surface

Plasma treatment of the substrate surface was performed using a TePla 440 plasma system with an airflow of 170 l/min and power of 480 W for 3 minutes. The plasma treatment was done on Julien 1, the TPE substrate without any hydrophilic additive, and Julien 4, the TPE-substrate with a hydrophilic additive. The contact angle of each substrate was then measured.

3.2.4 Drop Casting

Initial screening of GNFs deposition was performed by applying a total volume of 50 μl of A1 and A2 dispersions on 1 cm^2 samples of Julien 1 and Julien 4 that were both non-treated and plasma treated to evaluate wetting, spreading, film formation and evaporation time of the diluted dispersions.

3.3 Surface Characterisation

3.3.1 Scanning Electron Microscopy

SEM was used to analyze the morphology and topography of different surfaces. All specimen were smaller than 1 cm^2 and completely dry before placed on a pin stub with carbon tape. To avoid charge build-up on the non-conductive surface, the specimen were sputtered with gold using air-generated plasma for 60 seconds in vacuum. [66]. The specimen were then mounted on the stub and placed in the chamber for analysis. The images were taken with both SE-detector and BSE-detector.

3.3.2 AFM

AFM measurements of the GNFs coated surfaces were carried out by NTEGRA system in tapping mode from NT-MDT. A sample with an area smaller than 1 cm^2 was placed on a sample holder with double-sided tape. Data processing was performed using the Gwyddion software with first-order polynomial tilt correction.

3.4 Drop Casting on Samples sent for Laser Treatment

Results from the screening process indicated that Julien 2-4 had similar surface properties. To delimit the data, the experiments continued with Julien 1 and Julien 4. Two coated 25 cm^2 samples of Julien 1 and Julien 4 plates were prepared for laser treatment. For the Julien 1 sample, a surface pre-treatment with plasma was done for 3 minutes and then coated with a total volume of 1.3 ml of dispersion A1 in five layers, where each layer was dried with plasma treatment for 30-60 seconds. This gave a final surface density of 0.052 mg/cm^2 GNFs. The Julien 4 sample was not pre-treated and was coated with a total of 6 ml A1 diluted dispersion, where each layer dropped was 1 ml and was air dried for in total of 5 hours. This gave a final surface density of 0.24 mg/cm^2 deposited GNFs. Both were sent to Mid University Sweden where laser treatment was done. After the laser treatment, SEM-analysis was done to compare the surface topography. AFM was also conducted on the Julien 1 sample and one sample that was made in previous studies which had a surface density of 1 mg/cm^2 deposited GNFs by drop casting on a polypropylene (PP) film sheet, to compare how a high density of GNFs on the surface affects the final structure created by laser treatment.

Table 3.4: Overview of the final samples for laser treatment and AFM.

Material	Density of deposited GNFs (mg/cm^2)	Surface treatment
Julien 1	0.052	Plasma-treated
Julien 4	0.24	None
PP film	1	None

The lasered GNFs coated Julien 1 sample was then sent to Chalmers for antibacterial testing. Antibacterial testing was done using serial dilution and plating method to determine the reduction of *E. coli* and *S. aureus* on the surface compared to a non-lasered surface.

3.5 Pilot-scale Dip Coating Process

In preparation of the pilot-scale dip coating process, all materials were cleaned with ethanol and air dried. Flame treatment of the tubes and plates of the material Julien 1 was then done with two nozzles with a distance of 15 cm where the material passed the flames with a rate of 33 cm/s. The tubes and plates were then mounted on a

stand that was dipped with an automated robot in an A1 dispersion. After each dip, the tubes and plates were dried in a 70°C oven for five minutes, and the dip cycle was repeated 6 times to evaluate the uniformness of the coating.

3.6 Disclosure and Declaration of AI use

The AI tool Copilot was used for support in creating templates in Python programming language and LaTeX that were used to create tables, graphs and bar charts for presenting the results of the experiments.

4
Results and Discussion

4.1 Screening Process

4.1.1 Comparative Analysis of Julien 1-4

Contact angle measurements of Julien 1-4 with water as the liquid, showed that the materials with a hydrophilic additive in their polymer matrix (Julien 2-4) had similar contact angles that were much lower compared to the TPE material without a hydrophilic additive (Julien 1) as shown in Figure 4.1.

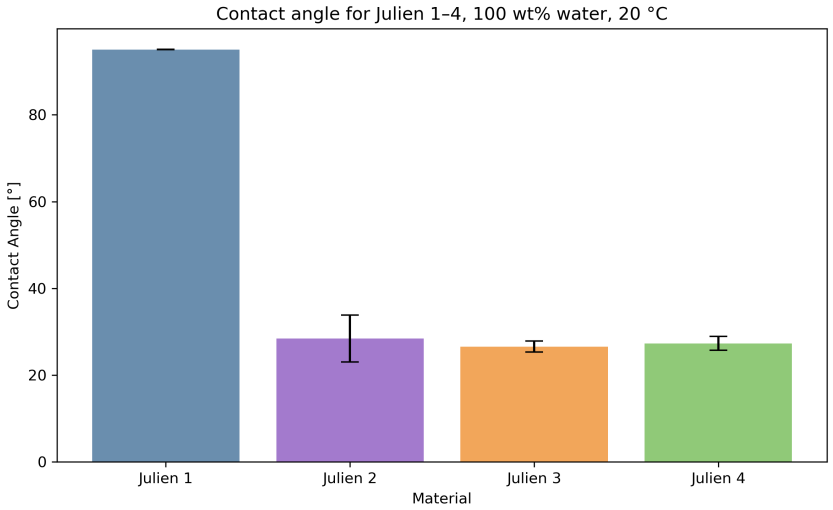

Figure 4.1: Contact angle measurements of water on Julien 1-4

This may be due to the hydrophilic additive migrating to the surface of the polymer which increases the surface energy [44] [47]. The small differences between the contact angles of Julien 2-4 may be due to the different additives or the TPE formulations, or it could be due to small variations in droplet mass which are effected by the gravitational force [63], lowering the contact angle.

Measurements of the four different roughness parameters Ra, Rdc, RSm and RPc of the different materials Julien 1-4 plates, seen in figure 4.2, showed that the four materials had similar roughness profiles on their rough side.

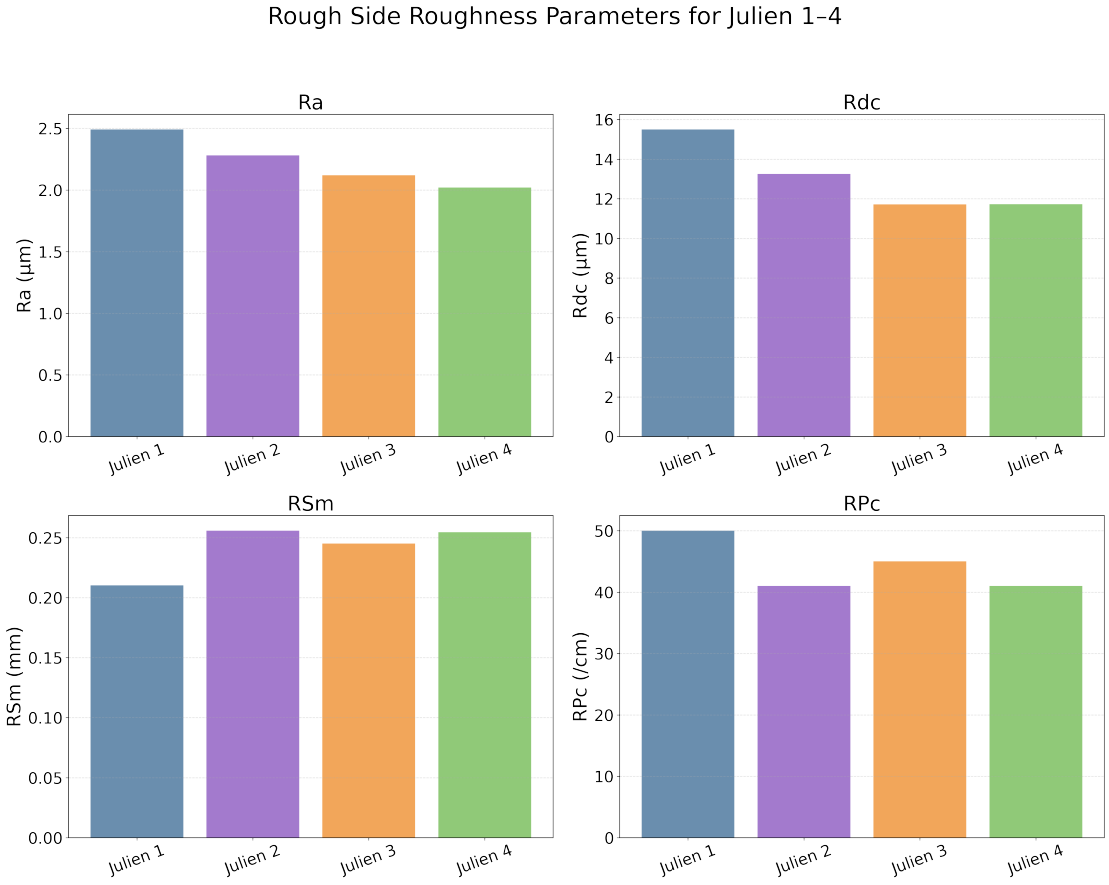

Figure 4.2: Roughness parameters of the different TPE materials Julien 1-4 rough side.

This may be due to the materials having the same processing method [40]. The roughness of these materials being so similar indicates that its not a main factor affecting their wetting results.

4.1.2 Comparative Analysis Between Plates Rough side, Smooth side and Tubes

The mean of the roughness parameter values, Ra, Rdc, RSm and RPc obtained from measurements done on Julien 1-4 plates rough side, Julien 1-4 plates smooth side and Julien 1-4 tubes are shown in Figure 4.3. The roughness values of Julien 3 smooth side could not be measured. This may have been to surface being too smooth or the additive on the surface disturbing the measurement. Ra values of the plates rough side compared to the tubes are very similar and both relatively higher

than then the Ra values of the smooth surfaces and show that the average roughness of the tubes and rough side of the plates are similar.

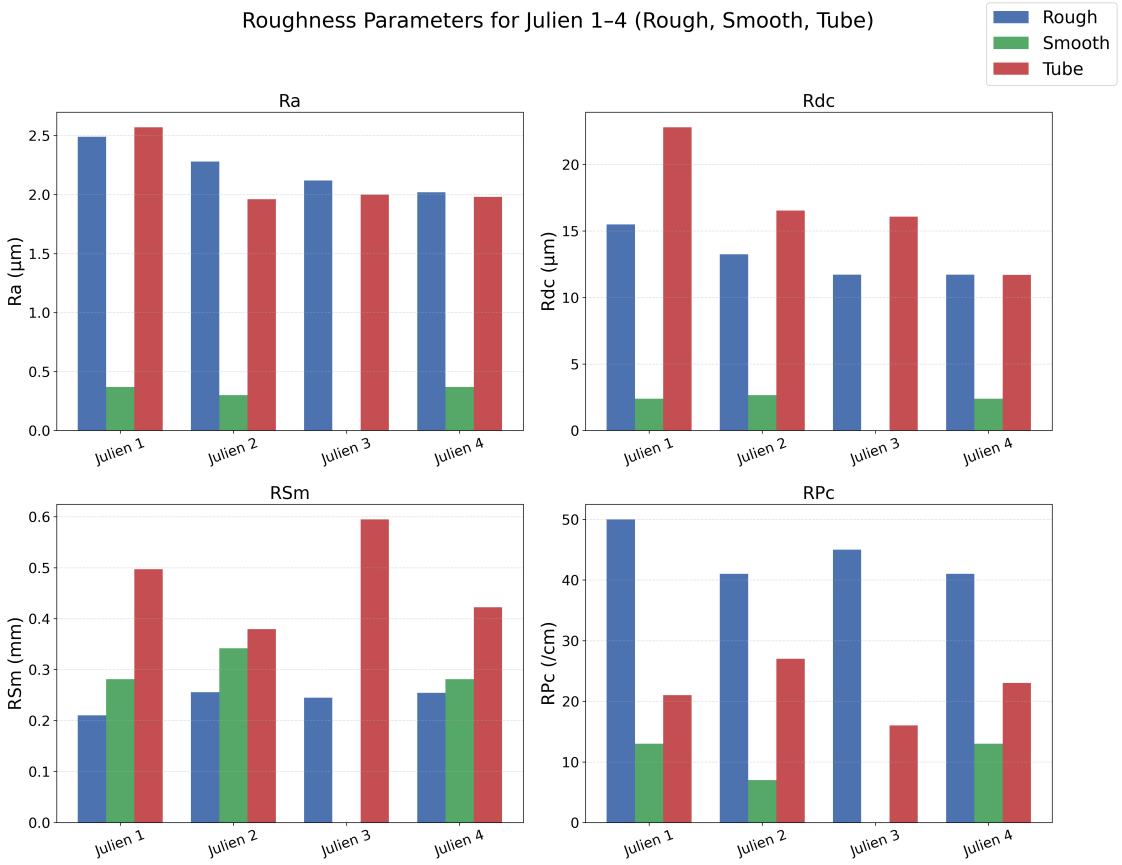

Figure 4.3: Mean roughness parameters of Julien 1-4 plates rough and smooth side compared to the tubes.

The Rdc value, which represented the depth of the main roughness structure or the "valleys" of the surface [61][62], is higher for the tubes, however the rough side of the plates are much closer to the tubes Rdc value compared to the smooth side of the plates. The rough side of the plates have the highest RPc and lowest RSm value, indicating many bumps with small spacing [61][62]. The tubes have the highest RSm value and a RPc value half the value of the rough side but double the value of the smooth side, meaning more bumps than the smooth surface, but less bumps compared to the rough side and higher spacing between the bumps than both. The smooth surface have the lowest RPc value, fewer peaks per unit length but a smaller spacing compared to the tubes. In Figure 4.4 there is a SEM picture of a) Julien 1 rough side of the plate and b) Julien 1 tube.

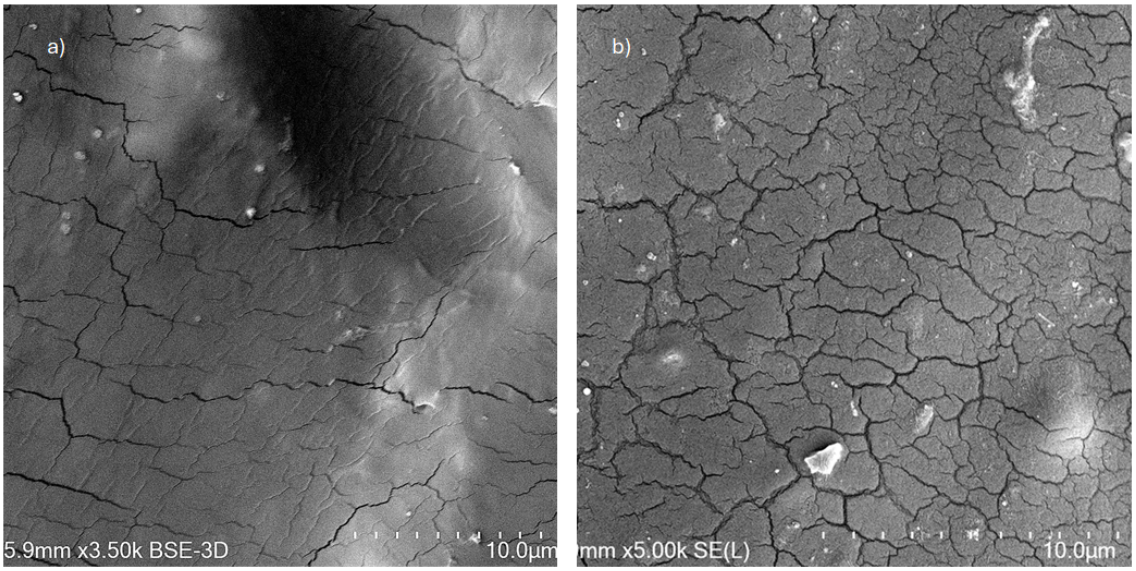

Figure 4.4: SEM-Images of a) Julien 1 rough side of plate and b) Julien 1 tube without any GNFs coating.

The surfaces have similarities showing cracks in both surfaces that may be due to the processing of the TPE. The plate surface structure differs however in the topography showing more bumps compared to the tube, which is in accordance with the RPc value seen in Figure 4.3. Based on the results displayed in Figure 4.3 and Figure 4.4, the rest of the experiment was performed on the rough side of the plates as they were comparable to the tubes.

4.1.3 The Optimal Dispersion

4.1.3.1 Water-Ethanol Ratio

The images in Table 4.1 show that ethanol wets the surface of non-treated Julien 1 and Julien 4 better than water. Ethanol has a hydrophilic and hydrophobic part in its molecular structure giving it surfactant attributes [52][54] which may lower the surface tension between the hydrophobic solid surface and water. Water molecules have strong hydrogen bonding forces in its bulk [54], and weaker interactions with air and hydrophobic surfaces like Julien 1. This makes water change its shape to the lowest possible surface area on the same volume [46], creating spherical droplets.

Table 4.1: Contact angle measurement of Julien 4 and Julien 1 with 100 wt% water in the droplet and 100wt% ethanol

Material	100wt% Water	100wt% Ethanol
Julien 1	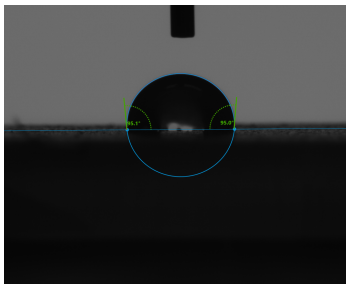	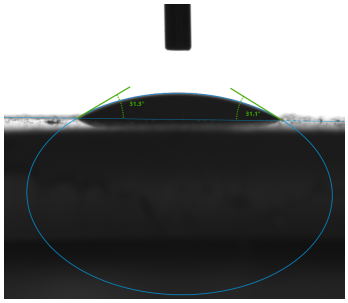
Julien 4	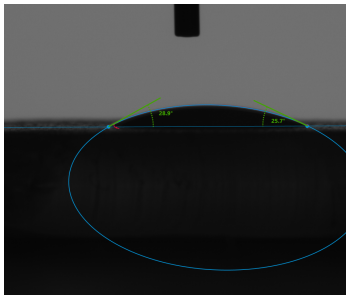	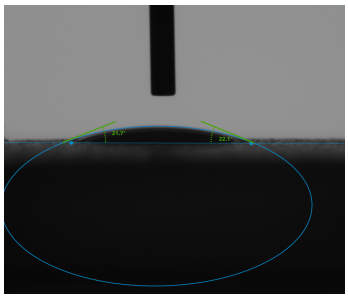

By mixing water with ethanol, the surface wetting increases as seen in Figure 4.5. An increased wt% ethanol decreases the contact angle for both Julien 1 and Julien 4. The greatest reduction of contact angle was for Julien 1, with a relatively large difference between 56 wt% and 70 wt% ethanol.

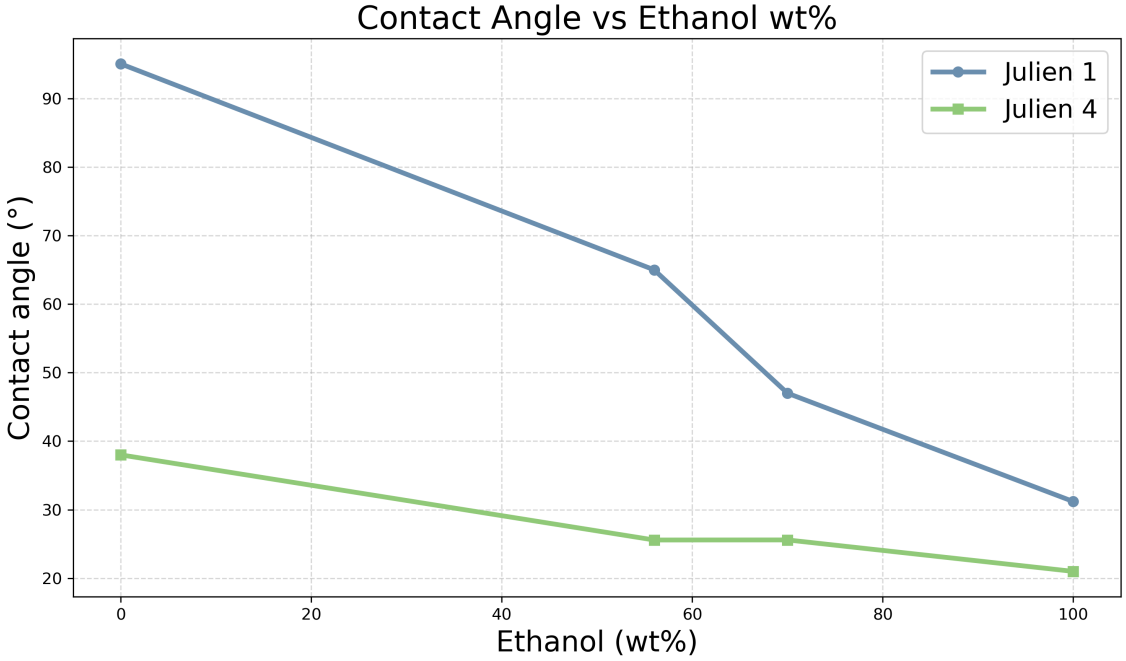

Figure 4.5: Contact angle against increased wt% of ethanol where 0 wt% ethanol is 100 wt% water and vice versa.

The hydrophilic surface of the Julien 4 sample showed a decrease of half its contact angle between 0 wt% and 100wt% and almost no difference between 56 wt% and 70 wt% ethanol. This may be due to the hydrophilic additive not covering the whole surface leaving hydrophilic and hydrophobic regions. The Julien 4 surface has less hydrophobic regions then Julien 1 and therefore less surface tension to lower, which may explain the difference of the total reduction in contact angle. However, the final contact angle was still lower for Julien 4 than Julien 1.

4.1.3.2 Concentration of GNFs in Dispersion

As shown in Figure 4.5, increased ethanol wt% lowered the contact angle, hence lowered the surface tension between the liquid and solid surface of both TPE materials Julien 1 and Julien 4. The effect of increased ethanol wt% and lowered GNFs concentration in the diluted dispersion is shown in Figure 4.6 where three samples of Julien 4 with no pre-treatment was coated with the drop coating method.

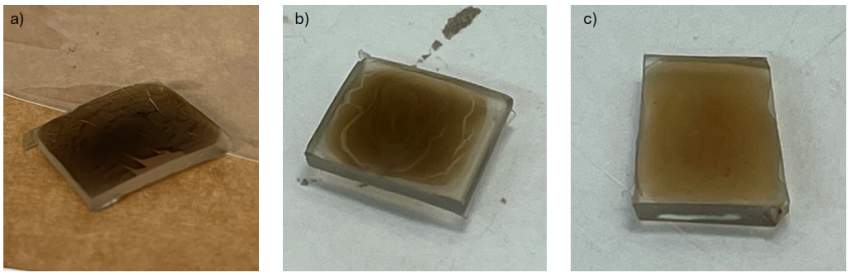

Figure 4.6: Drop casting done on three 1 cm^2 pieces of Julien 4 with 50 μl of the three different dispersions a)A: 4mg/ml b) A2: 2mg/ml c) A1: 1mg/ml

In Figure 4.6a) the coating is relatively thick compared to the coatings in Figure 4.6b) and 4.6c) which is due to larger density of GNFs deposited. In Figure 4.6b) the coating is not homogeneous and it appears to have occurred aggregation of GNFs before the solution evaporated, leaving cracks and a coating that is still adhered to the surface. In Figure 4.6c) the coating looks more homogeneous. The large cracks in the coating and detachment from the surface observed in Figure 4.6a) may be due to the GNFs coating being adhered to the hydrophilic additive on the surface, not the actual surface. Because the additive is not crosslinked to the polymer matrix, it can migrate to the surface, creating a layer between the coating and the substrate surface. If the additive layer is thick enough, the GNFs coating may only be adhered to the additive, making the coatings attachment to the TPE dependent on the additives presence on the surface. However, if that was the reason to the detachment, it would also be observable in Figure 4.6b) and c). The cracks and detachment could possibly still exist in the thinner coatings but is more visible for thicker coatings. GNFs are more brittle materials compared to TPE materials, therefore cannot accommodate the TPE materials deformation and flexibility. The cracks may also occur due to the already existing cracks in the TPE materials surface.

4.1.4 Surface Treatments of Hydrophobic Surfaces for Homogeneous Deposition of GNFs

Contact angle measurements of Julien 1 and Julien 4 with plasma- and flame-treated surfaces were obtained and compared to their non-treated surface contact angles as shown in Figure 4.7.

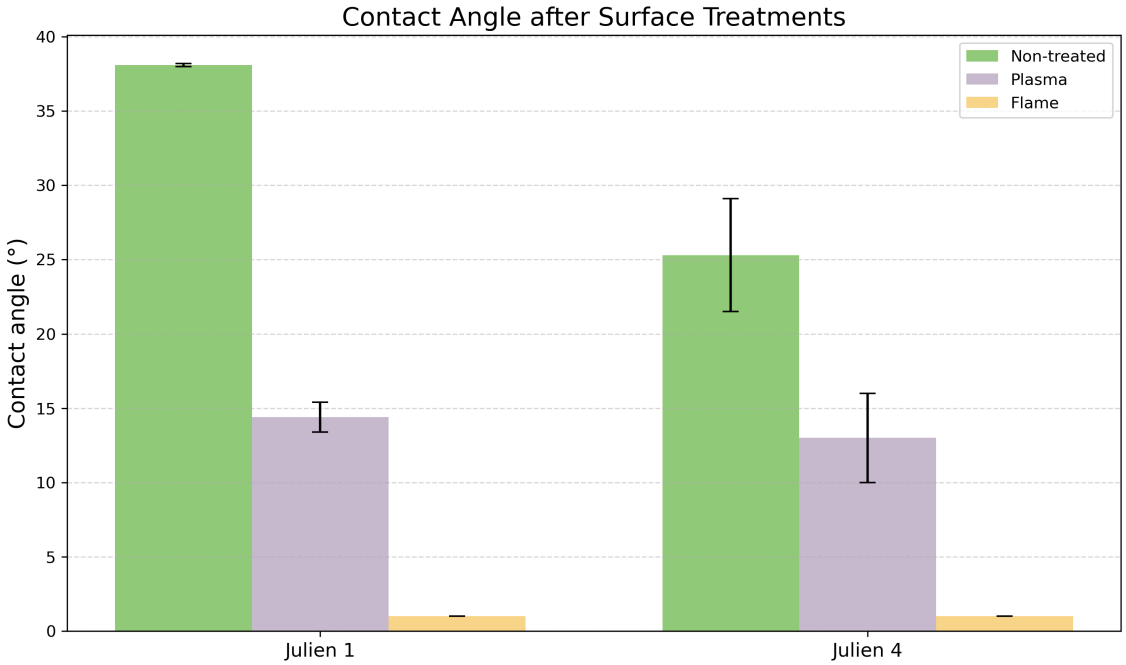

Figure 4.7: Contact angle measurements of Julien 1 and Julien 4 with 30/70 water/ethanol (wt%).

Flame treatment showed the highest reduction of contact angle. Due to the limited availability of the flame treatment, it was not used as a pre-treatment before drop casting in the screening process. A plasma treatment of the hydrophobic surface of Julien 1 was done before the coating was dropped. In Figure 4.8, two pieces of Julien 1 are shown, where the sample in Figure 4.8a) is not pre-treated and the GNFs coating is concentrated in the middle and fades out on the edges.

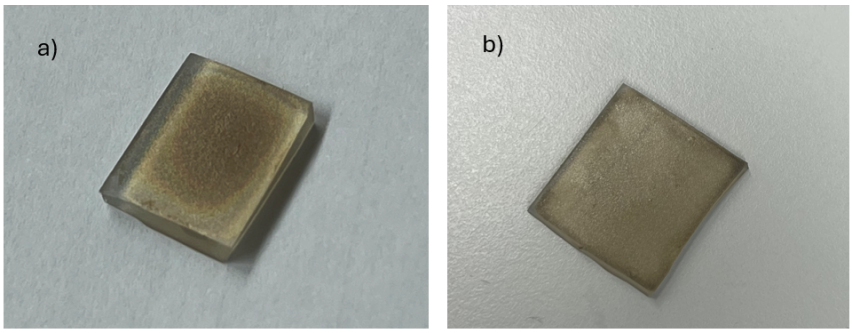

Figure 4.8: Two 1 cm^2 Julien 1 plates that are a) coated with GNFs drop-casting method without plasma treatment b) pre-treated with plasma and then coated with GNFs by dropcasting method

This effect may occur due to the surface having low surface energy [58] and the dropped dispersion creates a droplet on the surface with high contact angle which concentrates the GNFs deposition in the center, where the droplet was. In Figure 4.8b) the sample was pre-treated with plasma and shows an even distribution of deposited GNFs on the surface after drop casting. This is due to the plasma treatment increasing the surface energy of the polymer by adding oxygenated functional groups to the surface [37][48], increasing wetting of the dispersion dropped on the surface which leads to a homogeneous liquid film over the surface, hence a homogeneous deposition of GNFs. The oxygen functional groups that are present on the surface after the plasma treatment may also alow for the GO nanoflakes to hydrogen bond to the surface and increase the coating adhesion.

4.2 Final Drop Casting

Results obtained from the screening process led to the choice of materials Julien 1 and Julien 4 and a diluted dispersion A1, with a concentration of 1mg/ml GNFs in a solvent with 70 wt% ethanol and 25 wt% water. The combination of the hydrophobic TPE, Julien 1, and a plasma treatment made the diluted dispersion A1 wett the surface well and gave a uniform coating. Julien 4, with no pre-treatment and the same diluted dispersion also showed an even distribution of GNFs. The coating on the Julien 1 sample was much thinner compared to the coating of Julien 4 because of more layers of deposited GNFs. In Figure 4.9, SEM images of Julien 1 with and without coating are shown. In Figure 4.9a) the bare surface is shown, which has bumps and cracks in its structure and in Figure 4.9c) a higher magnification of the bare surface is shown. In Figure 4.9b) and c) the GNFs coating is shown from the top view and side view with different magnifications.

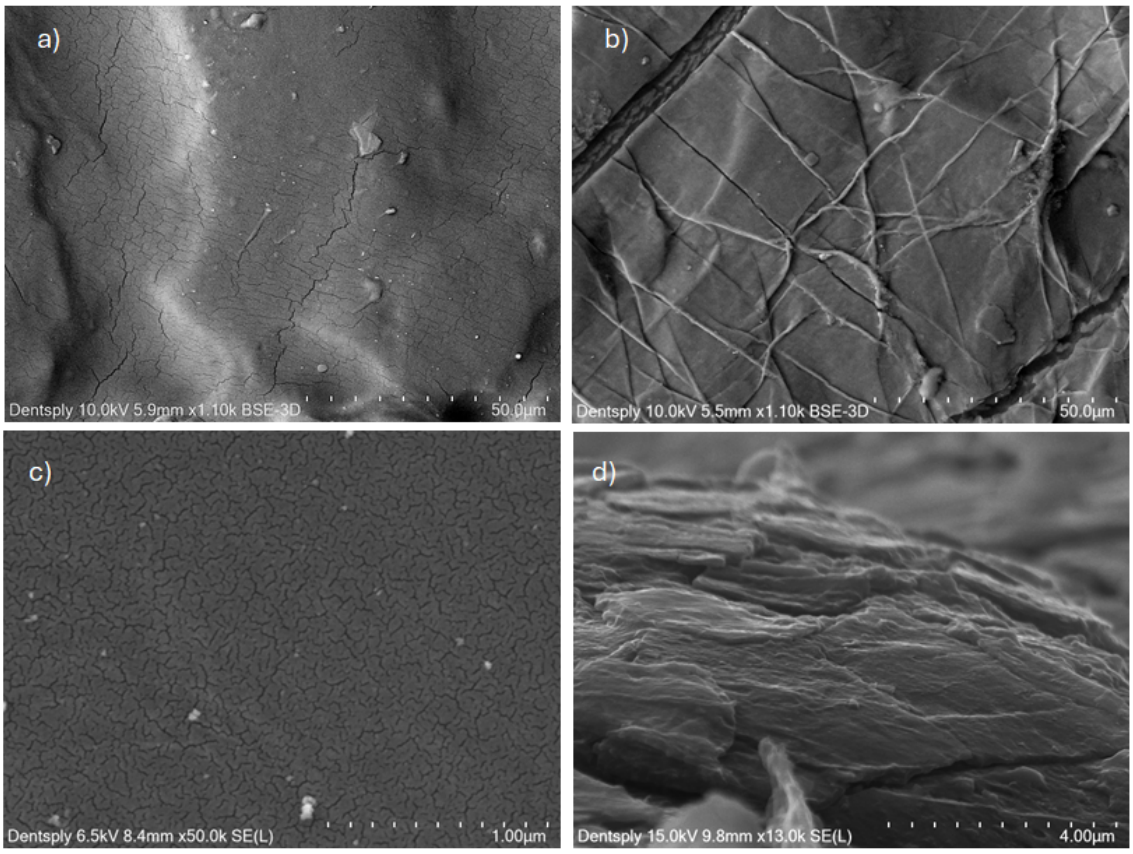

Figure 4.9: SEM-images of a) Julien 1 plate surface without coating b) Julien 1 with GNFs Coating top view c) Julien 1 surface without coating and d) side view of Julien 1 coated with GNFs.

The wrinkly structure of the coating is observable in Figure 4.9b) where cracks are also visible. The creases in the structure are due to the out-of-plane deformations in the GNFs [34]. Observing the coating from the side shows how the flakes lie horizontally on top of each other with lateral size matching the ones in table 3.2 and also showing the high aspect ratio of the flakes.

4.3 Laser Treatment

The results obtained from the laser treatment of the GNFs coated samples were analyzed with SEM. A comparison between two samples with different GNFs density on the surface but same laser parameters was done and also compared to an old sample with the highest density from a previous study. 3D-images of the samples with lowest surface density and highest surface density of GNFs were obtained from AFM showing the topography of the structures obtained from laser exposure.

4.3.1 The Effect of GNFs Coating Density

The surfaces with the most deposited GNFs by drop casting showed more tendency to crack and detach from the surface, as shown in Figure 4.10 compared to the

less dense coatings. In Figure 4.10, three SEM pictures are shown of laser exposed GNFs coating. Figure 4.10a) shows a laser-exposed surface of the PP film sample with GNFs surface density of 1mg/1 cm^2. Figure 4.10b) displays the laser exposed coating surface of the Julien 1 sample with GNFs surface density of 0.052 mg/1 cm^2 and in 4.10c) a Julien 4 sample with GNFs surface density of 0.24 mg/1 cm^2 is displayed where both 4.10b) and c) have a scale bar of 20 μm and were made with the same laser parameters to create these structures. Figure 4.10a) has a scale bar of 10 μm, displaying a more zoomed in area.

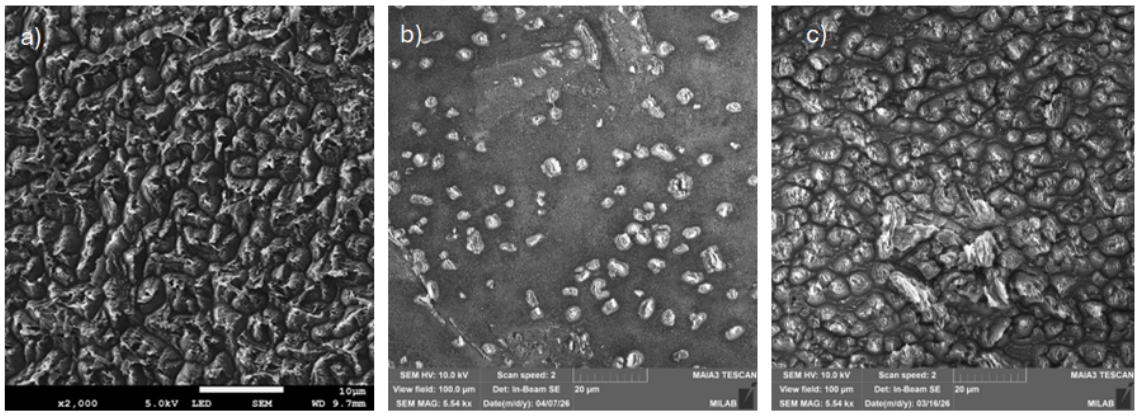

Figure 4.10: SEM-images of Laser exposed GO coated polymer surfaces with different densities of deposited GNFs. a) old sample from previous studies with a surface density of $1mg/cm^2$ b) Julien 1 with a surface density of $0.052mg/cm^2$ c) Julien 4, with a surface density of $0.24mg/cm^2$.

In all pictures, a mountain looking structure is observed. Each mountain may display a clump of GNFs standing vertically on the polymer surface due to the laser, or just a structure created on the coating. In Figure 4.10a) and c) the structures look very similar, with a dense mountain structure, and lateral sizes of each individual mountain in both pictures range in the same size region, but may have a lateral size too large to pierce a bacteria. However, the tip of the mountains looks like multiple sharp blades and not a flat surface which could give an antibacterial effect. In Figure 4.10b) We see the mountain structure but less dense compared to the other two, which likely is due to the density of the deposited GNFs prior to laser exposure being less than the other to samples. However, Figure 4.10c) shows that in comparison to 4.10a) almost the same structure can be achieved but with less amount of GNFs on the surface. Higher surface density of deposited GNFs give a darker coating, which may increase the absorbance of laser. This may allow for easier creation of structures of the coating. The regions without vertical GNFs mountains in Figure 4.10b) are shown in Figure 4.11. The scale bar is 10 μm for the top picture in 4.11 where a structure of what looks like single fragments of the GNFs are placed vertically on the polymer surface. The bottom left and right SEM-image in Figure 4.11 show regions with a scale bar of 1 μm.

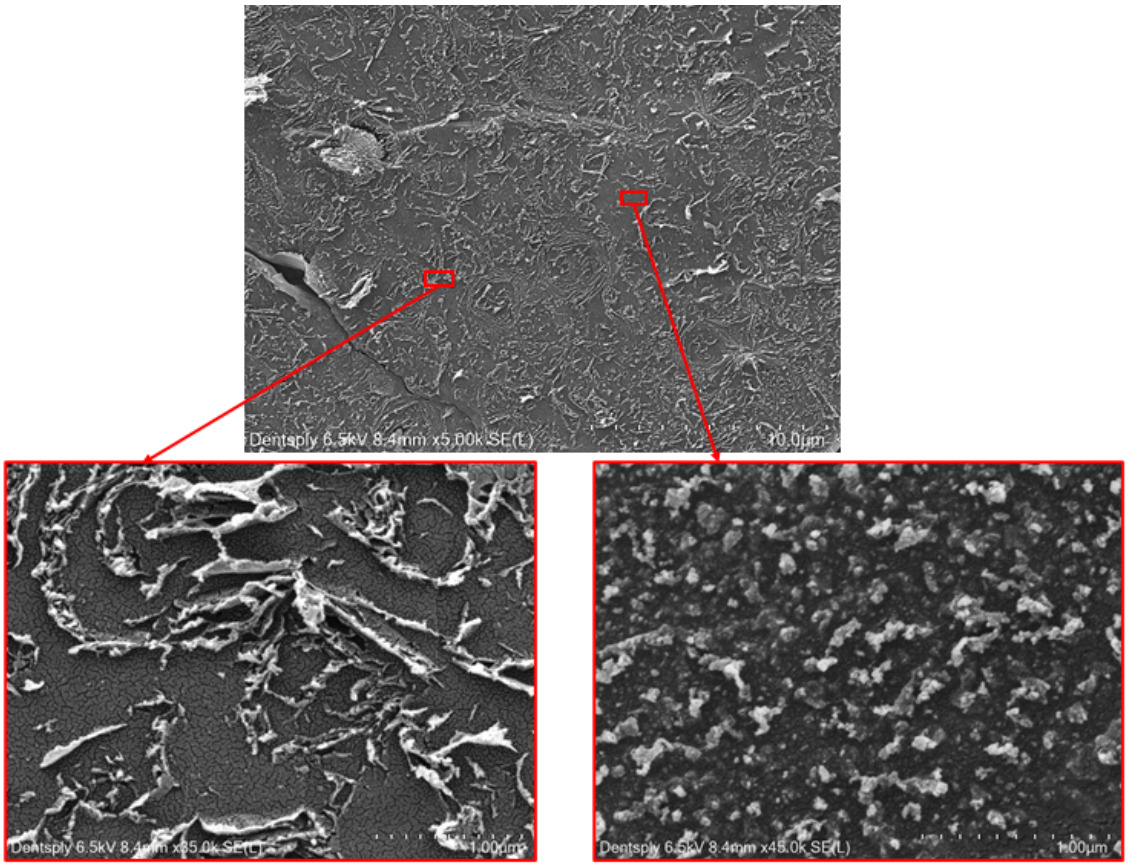

Figure 4.11: Structure of Julien 1 sample after laser treatment in less GNFs dense regions. The red rectangles do not represent a true scale.

In Figure 4.11 bottom left picture, the regions seen in between the GNFs fragments looks like the surface structure seen in 4.9c) of the bare substrate surface without any coating where the spacings between the fragments are 1-2 μm. In the bottom right picture in Figure 4.11, the structure is less sharp looking and could be melted polymer where the laser burnt away the little coating that was there and melted the surface. The lasered GNFs coating shown in 4.10a) and b) was also analyzed with an AFM and is shown in Figure 4.12a) and b).

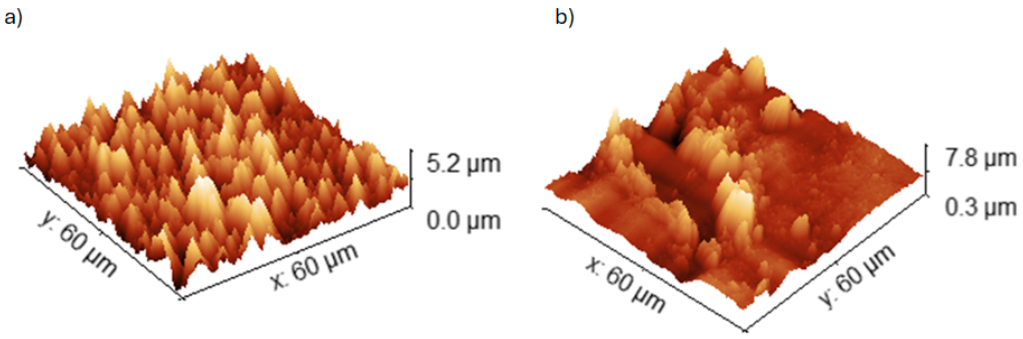

Figure 4.12: 3D-images from AFM showing a) the structure of the lasered coating on the PP film and b) the structure of lasered coating on the Julien 1 sample.

The scale of the AFM images in Figure 4.12 is comparable to the SEM-images in Figure 4.10. From Figure 4.12 a), the dense mountain structure seen is in accordance with the Figure 4.10 a) and the tip of the "mountains" has a top height of 5.2 μm which is in the range of the lateral sizes from table 3.2. In Figure 4.10 b) the peaks are fewer and less dense showing a top height of 7.5 μm, which also is in the range of the lateral sizes from table 3.2.

4.3.2 Antibacterial Testing on Lasered Thinner Drop Casted GNFs Coating

The lasered GNFs coated Julien 1 sample with a surface density of 0.052g/1 cm^2 deposited GNFs was tested for antibacterial effect at Chalmers with two different bacteria, *E. coli* and *S. aureus* and SEM-images of the antibacterial tested sample is shown in Table 4.2.

Table 4.2: SEM-images of bacteria film formation on lasered and non-lasered regions of GNFs coated Julien 1.

Bacteria	Non-Lasered	Lasered	Lasered
No Bacteria	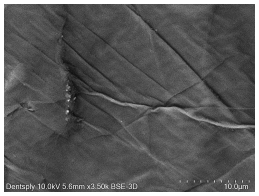	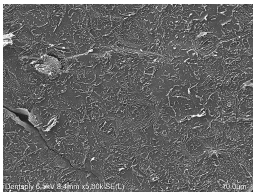	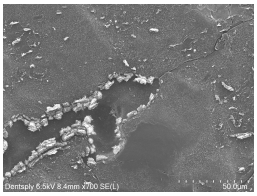
E. coli	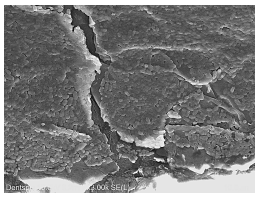	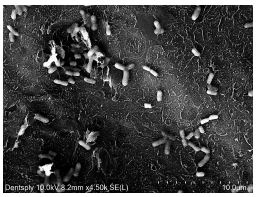	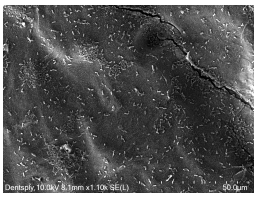
S. aureus	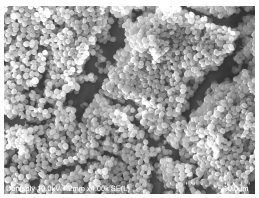	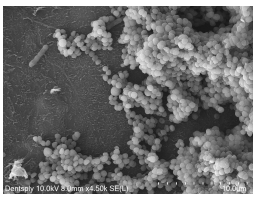	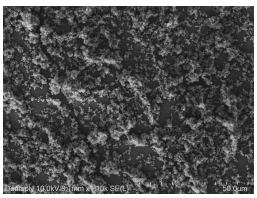

Bacterial growth on both lasered and non-lasered region is observed, however *S. aureus* have a greater bacterial growth compared to *E. coli* in both types of regions. This may be due to *E. coli* having a higher aspect ratio and being a gram-negative bacteria, making it larger than *S. aureus* in one direction and easier is caught between two GNFs [4][6]. *E. coli* also has a thinner layer of peptidoglycan in its cell wall [8] and therefore may be more vulnerable for sharp structures such as GNFs vertically aligned on a polymer surface. A reason for this observed bacterial growth may be due to the distance between the vertically aligned GNFs being too large, leaving space for the bacteria to attach to the polymer surface and multiplying and creates a biofilm leading to a loss of anti-fouling effect. For less bacterial growth, a denser vertically aligned GNFs structure like the one in Figure 4.10a) may be needed. These images also show that non-lasered regions, where the GNFs are horizontally aligned, show no antibacterial effect.

4.4 Dip Coating Pilot-scale Process

The results from the dip coating pilot-scale process showed that a homogeneous coating of GNFs on the catheter tubes is achievable by combining flame treatment, Julien 1 material and the diluted dispersion A2. Two Julien 1 catheter tubes that were dipped 6 times are shown in 4.13 where there is a clear boundary between the coated and non-coated area.

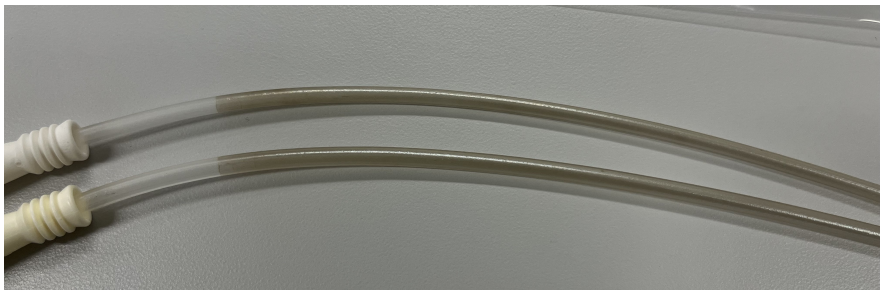

Figure 4.13: Julien 1 catheter tubes after dip coating pilot process.

This shows that the dip-coating process was controlled and gave a homogeneous deposition of GNFs on the tubes. Due to the time limit, the process parameters were not explored, and may not have been optimal for a further scale up process. Each cycle, which included dipping and withdrawing the tubes with specific rates, stay time in the dispersion and drying time in the oven, was time consuming. To reduce the time of the cycles and the overall process, different parameters should be analyzed, including the concentration of GNFs of the diluted dispersion as the same results may be achieved with fewer dip-cycles. The boundary between the coated and non-coated area was analyzed with SEM and is shown in Figure 4.14 where the contrast between the wrinkly coating structure seen in previous results and the bare polymer tube surface with cracks is displayed.

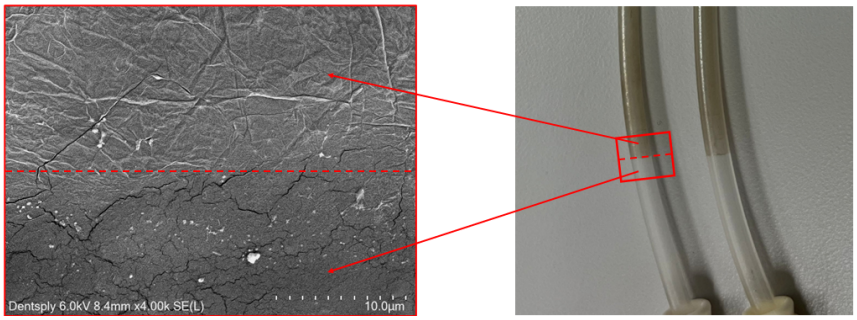

Figure 4.14: SEM-image of the boundary between the GNFs coating and Julien 1 tube bare surface.

The Julien 1 plates were also dip coated in the same process as the Julien 1 tube for the purpose of sending them to the Mid University where finding the right laser parameters would be performed on the plates and then applied on the tubes. When comparing the coating structure with SEM for a tube and plate with the same amount of dipping cycles, the structure is not exactly the same. However the wrinkly structure is obsereved in both as shown in 4.15.

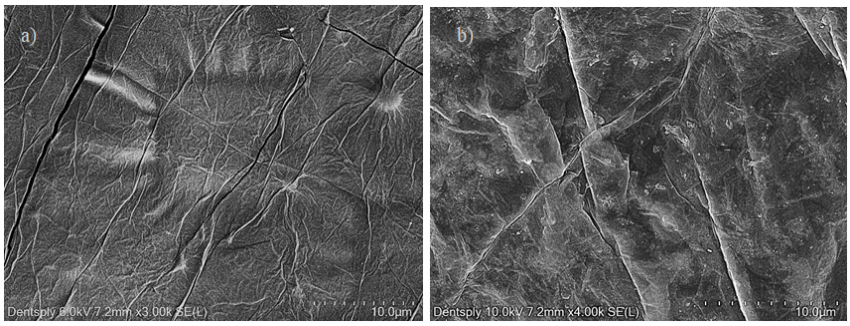

Figure 4.15: Comparison of the GNFs coating achived by dip coating of a) Julien 1 tube b) Julien 1 plate

Figure 4.15a) shows the structure of the coating on the tube which has visible cracks in the structure, which is something also seen in the results from the drop casting method. This indicates that the methods are not the main factor for the cracks but may be an intrinsic property of GNFs coatings. Or the cracks in the coating may be due to the polymer surface already having cracks as displayed in Figure 4.4. Figure 4.15b) shows the coating of the dipped plates, which also shows visible cracks.

5
Conclusions

5.1 Screening Process

The findings from the screening process showed that the three TPE materials Julien 2-4 with a hydrophilic additive in their polymer matrix had higher surface energy compared to the material without any additive. After the flame and plasma treatments of Julien 1, the wetting of the surface was approximately the same as plasma treated Julien 4. Plasma and flame treated Julien 1 had higher surface energy than non-treated Julien 4. The obtained roughness parameter values from the profilometer showed that the relatively rougher side of Julien 1-4 plates showed very similar results to each other and the tubes from the same materials. SEM-images comparing the surface of the bare Julien 1 tube and plate showed that they had a similar structure with cracks. From this it was concluded that the rest of the experiment could be performed on the rough side of the plates as they are comparable to the tubes. The main difference between the materials Julien 1-4, was that Julien 2-4 had a hydrophilic additive increasing the surface energy without any plasma or flame treatment. To narrow down the data obtained, the final drop casting was done with Julien 1 plates combined with plasma and flame treatment and non-treated Julien 4 plates.

Results from exploring the optimal diluted GNFs dispersion parameters, with cheap and scalable materials, showed that the green solvents water and ethanol, proved effective for deposition of GNFs on a polymer substrate using the drop casting and dip coating methods. The screening of different wt% of water and ethanol for the dispersion of GNFs showed that 30wt% water/70wt% ethanol gave relatively good wetting results while still allowing a reasonable concentration of GNFs. The sample with the lowest density of deposited GNFs on the polymer surface gave less visible cracking and detachment of the coating from the polymer surface on macroscale but visible cracks in the SEM-images.

5.2 Density of Drop Casted GNFs and Dip Coating Pilot-scale Process

SEM analysis of three laser-treated samples with different densities of deposited GNFs showed that the two samples with higher density gave a more dense peaky structure of vertically aligned GNFs on the surface compared to the one with the lowest density, which was also confirmed with AFM. The sample with a surface density of 1mg/cm^2 had a similar structure to the one with the surface density 0.24 mg/cm^2, meaning a peaky and dense structure can be achieved by laser with less GNFs. This creates a window between 0.052 mg/cm^2 and 0.24 mg/cm^2 that should be further studied to see what the lowest density of GNFs on a polymer surface achieves the same dense and peaky structure after laser treatment. SEM analysis of the less peak dense regions of the lasered sample with 0.052 mg/cm^2 GNFs on the polymer surface showed a structures that may have been fragments of single flakes and melted polymer. The antimicrobial testing of the less dense coating showed biofilm formation in both non-lasered and lasered regions the bacteria *E. coli* and *S. aureus*. This may be due to the vertically aligned GNFs not being dense enough or sharp enough, creating space for the bacteria to attach to the surface. The antibacterial effect results from SEM should be combined with CFU count for a quantitative result and be compared to the antibacterial effect of the lasered denser GNFs coatings for future research. The dip coating pilot-scale process showed that homogeneous deposition of GNFs on medical devices like catheter tubes is achievable. The process parameters should be explored and further optimized for an effective process in future studies.

Bibliography

[1] Benedetta Allegranzi et al. *Report on the burden of endemic health care-associated infection worldwide*. Geneva: World Health Organization, 2011.

[2] C Mosconi et al. "Costs and control strategies of healthcare-associated infections in an Italian university hospital". In: *European Journal of Public Health* 33.Supplement_2 (Oct. 2023). ISSN: 1101-1262. DOI: 10.1093/eurpub/ckad160.747.

[3] N. Sharmila Devi et al. "Overview of antimicrobial resistance and mechanisms: The relative status of the past and current". In: *The Microbe* 3 (June 2024), p. 100083. ISSN: 29501946. DOI: 10.1016/j.microb.2024.100083.

[4] Glenn T Werneburg. "Catheter-Associated Urinary Tract Infections: Current Challenges and Future Prospects". In: *Research and Reports in Urology* Volume 14 (Apr. 2022), pp. 109–133. ISSN: 2253-2447. DOI: 10.2147/RRU.S273663.

[5] Carol E. Chenoweth, Carolyn V. Gould, and Sanjay Saint. "Diagnosis, Management, and Prevention of Catheter-Associated Urinary Tract Infections". In: *Infectious Disease Clinics of North America* 28.1 (Mar. 2014), pp. 105–119. ISSN: 08915520. DOI: 10.1016/j.idc.2013.09.002.

[6] Mansel. Griffiths. *Understanding pathogen behaviour : virulence, stress response, and resistance*. CRC Press : Cambridge, England : Woodhead, 2005, p. 611. ISBN: 9781855739536.

[7] Raghad H.F. Bashabsheh et al. "Staphylococcus aureus epidemiology, pathophysiology, clinical manifestations and application of nano-therapeutics as a promising approach to combat methicillin resistant Staphylococcus aureus". In: *Pathogens and Global Health* 118.3 (Apr. 2024), pp. 209–231. ISSN: 2047-7724. DOI: 10.1080/20477724.2023.2285187.

[8] L. Pasquina-Lemonche et al. "The architecture of the Gram-positive bacterial cell wall". In: *Nature* 582.7811 (June 2020), pp. 294–297. ISSN: 0028-0836. DOI: 10.1038/s41586-020-2236-6.

[9] Claire Maher and Karl A. Hassan. "The Gram-negative permeability barrier: tipping the balance of the in and the out". In: *mBio* 14.6 (Dec. 2023). ISSN: 2150-7511. DOI: 10.1128/mbio.01205-23.

[10] Rania G Elbaiomy et al. "Antibiotic Resistance: A Genetic and Physiological Perspective." In: *MedComm* 6.11 (Nov. 2025), e70447. ISSN: 2688-2663. DOI: 10.1002/mco2.70447.

[11] Shyamalima Saikia and Pankaj Chetia. “Antibiotics: From Mechanism of Action to Resistance and Beyond.” In: *Indian journal of microbiology* 64.3 (Sept. 2024), pp. 821–845. ISSN: 0046-8991. DOI: 10.1007/s12088-024-01285-8.

[12] Christopher J L Murray et al. “Global burden of bacterial antimicrobial resistance in 2019: a systematic analysis”. In: *The Lancet* 399.10325 (Feb. 2022), pp. 629–655. ISSN: 01406736. DOI: 10.1016/S0140-6736(21)02724-0.

[13] Santosh Pandit et al. “Vertically Aligned Graphene Coating is Bactericidal and Prevents the Formation of Bacterial Biofilms”. In: *Advanced Materials Interfaces* 5.7 (Apr. 2018). ISSN: 2196-7350. DOI: 10.1002/admi.201701331.

[14] Alexander Kromka et al. “Bacterial response to nanodiamonds and graphene oxide sheets”. In: *physica status solidi (b)* 253.12 (Dec. 2016), pp. 2481–2485. ISSN: 0370-1972. DOI: 10.1002/pssb.201600237.

[15] Xinglin Lu et al. “Enhanced antibacterial activity through the controlled alignment of graphene oxide nanosheets”. In: *Proceedings of the National Academy of Sciences* 114.46 (Nov. 2017). ISSN: 0027-8424. DOI: 10.1073/pnas.1710996114.

[16] Shadi Rahimi et al. “Automated Prediction of Bacterial Exclusion Areas on SEM Images of Graphene–Polymer Composites”. In: *Nanomaterials* 13.10 (May 2023), p. 1605. ISSN: 2079-4991. DOI: 10.3390/nano13101605.

[17] V. R. S. S. Mokkapati et al. “Bacterial response to graphene oxide and reduced graphene oxide integrated in agar plates”. In: *Royal Society Open Science* 5.11 (Nov. 2018), p. 181083. ISSN: 2054-5703. DOI: 10.1098/rsos.181083.

[18] Santosh Pandit et al. “Precontrolled Alignment of Graphite Nanoplatelets in Polymeric Composites Prevents Bacterial Attachment”. In: *Small* 16.5 (Feb. 2020). ISSN: 1613-6810. DOI: 10.1002/smll.201904756.

[19] Luong Xuan Duy et al. “Laser-induced graphene fibers”. In: *Carbon* 126 (Jan. 2018), pp. 472–479. ISSN: 00086223. DOI: 10.1016/j.carbon.2017.10.036.

[20] Kurtuluş Yılmaz et al. “Transfer of CVD-Graphene on Real-World Surfaces in an Eco-Friendly Manner”. In: *ACS Applied Engineering Materials* 1.8 (Aug. 2023), pp. 2042–2049. ISSN: 2771-9545. DOI: 10.1021/acsaenm.3c00211.

[21] Dimitrios A. Lamprou et al. “Polymeric Coatings and Their Fabrication for Medical Devices”. In: *Encyclopedia of Biomedical Engineering*. Elsevier, 2019, pp. 177–187. DOI: 10.1016/B978-0-12-801238-3.99869-6.

[22] Alessia Cabrini et al. “Ultrasonic spray deposition of PEGDE-crosslinked chitosan/graphene oxide coatings for enhancing gas barrier properties of polybutylene succinate films”. In: *Progress in Organic Coatings* 183 (Oct. 2023), p. 107760. ISSN: 03009440. DOI: 10.1016/j.porgcoat.2023.107760.

[23] Yin-Fen Ma et al. “Review of roll-to-roll fabrication techniques for colloidal quantum dot solar cells”. In: *Journal of Electronic Science and Technology* 21.1 (Mar. 2023), p. 100189. ISSN: 1674862X. DOI: 10.1016/j.jnlest.2023.100189.

[24] Archana Kaliyaraj Selva Kumar et al. “A mini-review: How reliable is the drop casting technique?” In: *Electrochemistry Communications* 121 (Dec. 2020), p. 106867. ISSN: 13882481. DOI: 10.1016/j.elecom.2020.106867.

[25] N.I. Zaaba et al. “Synthesis of Graphene Oxide using Modified Hummers Method: Solvent Influence”. In: *Procedia Engineering* 184 (2017), pp. 469–477. ISSN: 18777058. DOI: 10.1016/j.proeng.2017.04.118.

[26] Nargish Parvin et al. “Recent Advances in the Characterized Identification of Mono-to-Multi-Layer Graphene and Its Biomedical Applications: A Review”. In: *Electronics* 11.20 (Oct. 2022), p. 3345. ISSN: 2079-9292. DOI: 10.3390/electronics11203345.

[27] Syazwan Afif Mohd Zobir, Suraya Abdul Rashid, and Tongling Tan. “Recent Development on the Synthesis Techniques and Properties of Graphene Derivatives”. In: *Synthesis, Technology and Applications of Carbon Nanomaterials*. Elsevier, 2019, pp. 77–107. DOI: 10.1016/B978-0-12-815757-2.00004-8.

[28] Jamie H.. Warner et al. *Graphene : fundamentals and emergent applications*. Elsevier, 2013, p. 461. ISBN: 9780123945938.

[29] Małgorzata Krystek et al. “High-Performance Graphene-Based Cementitious Composites”. In: *Advanced Science* 6.9 (May 2019). ISSN: 2198-3844. DOI: 10.1002/advs.201801195.

[30] Xiao Wang et al. “Graphene Oxide-Based Polymeric Membranes for Water Treatment”. In: *Advanced Materials Interfaces* 5.15 (Aug. 2018). ISSN: 2196-7350. DOI: 10.1002/admi.201701427.

[31] A. Kuc, T. Heine, and G. Seifert. “Structural and electronic properties of graphene nanoflakes”. In: *Physical Review B* 81.8 (Feb. 2010), p. 085430. ISSN: 1098-0121. DOI: 10.1103/PhysRevB.81.085430.

[32] Li-Shang Lin et al. “Determination of the lateral size and thickness of solution-processed graphene flakes”. In: *Journal of Physics: Conference Series* 902 (Sept. 2017), p. 012026. ISSN: 1742-6588. DOI: 10.1088/1742-6596/902/1/012026.

[33] V. Castagnola et al. “Biological recognition of graphene nanoflakes”. In: *Nature Communications* 9.1 (Apr. 2018), p. 1577. ISSN: 2041-1723. DOI: 10.1038/s41467-018-04009-x.

[34] Jannik C. Meyer et al. “The structure of suspended graphene sheets”. In: *Nature* 446.7131 (Mar. 2007), pp. 60–63. ISSN: 0028-0836. DOI: 10.1038/nature05545.

[35] Amit Goswami, Suresh C. Pillai, and Gerard McGranaghan. “Surface modifications to enhance dropwise condensation”. In: *Surfaces and Interfaces* 25 (Aug. 2021), p. 101143. ISSN: 24680230. DOI: 10.1016/j.surfin.2021.101143.

[36] Lina Chen, Casey Yan, and Zijian Zheng. “Functional polymer surfaces for controlling cell behaviors”. In: *Materials Today* 21.1 (Jan. 2018), pp. 38–59. ISSN: 13697021. DOI: 10.1016/j.mattod.2017.07.002.

[37] S. Yoshida et al. “Surface modification of polymers by plasma treatments for the enhancement of biocompatibility and controlled drug release”. In: *Surface and Coatings Technology* 233 (Oct. 2013), pp. 99–107. ISSN: 02578972. DOI: 10.1016/j.surfcoat.2013.02.042.

[38] Bharat. Bhushan. *Modern tribology handbook*. CRC Press, 2001. ISBN: 9780849377877.

[39] Yuxuan Gong, Jian Xu, and Relva C. Buchanan. "Surface roughness: A review of its measurement at micro-/nano-scale". In: *Physical Sciences Reviews* 3.1 (Jan. 2018). ISSN: 2365-6581. DOI: 10.1515/psr-2017-0057.

[40] Simone Paggetti, Enrico Bedogni, and Paolo Veronesi. "Factors Affecting the Surface Roughness of the As-Built Additively Manufactured Metal Parts: A Review". In: *Metals* 15.10 (Sept. 2025), p. 1069. ISSN: 2075-4701. DOI: 10.3390/met15101069.

[41] C. Yang, U. Tartaglino, and B. N. J. Persson. "Influence of Surface Roughness on Superhydrophobicity". In: *Physical Review Letters* 97.11 (Sept. 2006), p. 116103. ISSN: 0031-9007. DOI: 10.1103/PhysRevLett.97.116103.

[42] Hao Chen, Xiaoping Li, and Dachao Li. "Superhydrophilic–superhydrophobic patterned surfaces: From simplified fabrication to emerging applications". In: *Nanotechnology and Precision Engineering* 5.3 (Sept. 2022). ISSN: 1672-6030. DOI: 10.1063/10.0013222.

[43] C. Mathew Mate and Robert W. Carpick. "Surface Roughness". In: *Tribology on the Small Scale*. Oxford University PressOxford, Aug. 2019, pp. 28–53. DOI: 10.1093/oso/9780199609802.003.0002.

[44] "Wetting and Wetting Agents, Hydrophobization and Hydrophobizing Agents". In: *Surface Chemistry of Surfactants and Polymers*. Wiley, Oct. 2014, pp. 377–390. DOI: 10.1002/9781118695968.ch20.

[45] Soo-Jin Park and Min-Kang Seo. "Solid-Liquid Interface". In: 2011, pp. 147–252. DOI: 10.1016/B978-0-12-375049-5.00003-7.

[46] Pierre-Gilles. De Gennes, Francoise. Brochard-Wyart, and David. Quere. *Capillarity and Wetting Phenomena : Drops, Bubbles, Pearls, Waves*. Springer New York, 2013, p. 298. ISBN: 9780387216560.

[47] Nikola Slepickova Kasalkova et al. "Wettability and Other Surface Properties of Modified Polymers". In: *Wetting and Wettability*. InTech, Dec. 2015. DOI: 10.5772/60824.

[48] Igor Levchenko et al. "Plasma and Polymers: Recent Progress and Trends". In: *Molecules* 26.13 (July 2021), p. 4091. ISSN: 1420-3049. DOI: 10.3390/molecules26134091.

[49] Klaus Reichardt and Luís Carlos Timm. "Water, the Universal Solvent for Life". In: *Soil, Plant and Atmosphere*. Cham: Springer International Publishing, 2020, pp. 7–13. DOI: 10.1007/978-3-030-19322-5{_}2.

[50] Binita Nanda et al. "Green solvents: A suitable alternative for sustainable chemistry". In: *Materials Today: Proceedings* 47 (2021), pp. 1234–1240. ISSN: 22147853. DOI: 10.1016/j.matpr.2021.06.458.

[51] Bushra Anees Palvasha et al. "Green solvents for soil and sediment remediation". In: *Green Sustainable Process for Chemical and Environmental Engineering and Science*. Elsevier, 2021, pp. 37–65. DOI: 10.1016/B978-0-12-821884-6.00013-9.

[52] Bradford H. Strohm and Leonard I. Sweet. “Ethanol”. In: *Encyclopedia of Toxicology*. Elsevier, 2005, pp. 263–266. DOI: 10.1016/B0-12-369400-0/00384-7.

[53] Karen Gaudin. “Potential of green solvents as mobile phases in liquid chromatography”. In: *Journal of Chromatography A* 1750 (June 2025), p. 465810. ISSN: 00219673. DOI: 10.1016/j.chroma.2025.465810.

[54] I. S. Ryzhkina et al. “Structure and Properties of Water–Ethanol Systems”. In: *Moscow University Chemistry Bulletin* 80.6 (Dec. 2025), pp. 375–383. ISSN: 0027-1314. DOI: 10.3103/S0027131425700403.

[55] William M.. Haynes, David R.. Lide, and Thomas J.. Bruno. *CRC handbook of chemistry and physics : a ready-reference book of chemical and physical data*. CRC Press, 2017. ISBN: 1498754287.

[56] Bruce H. Lipshutz and Sachin Handa. “Modernizing the 12 principles of green chemistry: it’s time”. In: *Green Chemistry* 28.13 (2026), pp. 5606–5612. ISSN: 1463-9262. DOI: 10.1039/D5GC05289K.

[57] *Fluoroplastics*. Elsevier, 2015. ISBN: 9781455731978. DOI: 10.1016/C2012-0-05998-4.

[58] Sina Ebnesajjad. “Fabrication Techniques For Fluoropolymers”. In: *Melt Processible Fluoroplastics*. Elsevier, 2003, pp. 449–507. DOI: 10.1016/B978-188420796-9.50017-5.

[59] Richard J Spontak and Nikunj P Patel. “Thermoplastic elastomers: fundamentals and applications”. In: *Current Opinion in Colloid & Interface Science* 5.5-6 (Nov. 2000), pp. 333–340. ISSN: 13590294. DOI: 10.1016/S1359-0294(00)00070-4.

[60] *Advanced Functional Polymers for Biomedical Applications*. Elsevier, 2019. ISBN: 9780128163498. DOI: 10.1016/C2018-0-00041-9.

[61] Georgios P. Petropoulos, Constantinos N. Pandazaras, and J. Paulo Davim. “Surface Texture Characterization and Evaluation Related to Machining”. In: *Surface Integrity in Machining*. London: Springer London, 2010, pp. 37–66. DOI: 10.1007/978-1-84882-874-2{_}2.

[62] International Organization for Standardization. *ISO 21920-2:2021 — Geometrical product specifications (GPS) — Surface texture: Profile — Part 2: Terms, definitions and surface texture parameters*. Tech. rep. Geneva: International Organization for Standardization, 2021. URL: https://www.iso.org/standard/72226.html.

[63] A. Arvay et al. “Characterization techniques for gas diffusion layers for proton exchange membrane fuel cells – A review”. In: *Journal of Power Sources* 213 (Sept. 2012), pp. 317–337. ISSN: 03787753. DOI: 10.1016/j.jpowsour.2012.04.026.

[64] Nidhi Raval et al. “Importance of Physicochemical Characterization of Nanoparticles in Pharmaceutical Product Development”. In: *Basic Fundamentals of Drug Delivery*. Elsevier, 2019, pp. 369–400. DOI: 10.1016/B978-0-12-817909-3.00010-8.

[65] A.D. Micheals. “Materials Analysis and Failure Analysis”. In: *Encyclopedia of Forensic Sciences*. Elsevier, 2013, pp. 483–493. DOI: 10.1016/B978-0-12-382165-2.00153-7.

[66] J. Webb and J.H. Holgate. “MICROSCOPY | Scanning Electron Microscopy”. In: *Encyclopedia of Food Sciences and Nutrition*. Elsevier, 2003, pp. 3922–3928. DOI: 10.1016/B0-12-227055-X/00779-3.

[67] Wanxin Sun. “Principles of Atomic Force Microscopy”. In: *Atomic Force Microscopy in Molecular and Cell Biology*. Singapore: Springer Singapore, 2018, pp. 1–28. DOI: 10.1007/978-981-13-1510-7{_}1.

[68] Ke Xu and Yuzhe Liu. “Studies of probe tip materials by atomic force microscopy: a review”. In: *Beilstein Journal of Nanotechnology* 13 (Nov. 2022), pp. 1256–1267. ISSN: 2190-4286. DOI: 10.3762/bjnano.13.104.

[69] Nuno C.. Santos and Filomena A.. Carvalho. *Atomic force microscopy : methods and protocols*. Humana Press, 2019, p. 372. ISBN: 9781493988945.

[70] James L. Suter and Peter V. Coveney. “Principles governing control of aggregation and dispersion of aqueous graphene oxide”. In: *Scientific Reports* 11.1 (Nov. 2021), p. 22460. ISSN: 2045-2322. DOI: 10.1038/s41598-021-01626-3.

A

Appendix A- Supplementary data

A.1 Roughness Profiles of Julien 1-4

Table A.1: Roughness profiles of a) Julien 1, b) Julien 2, c) Julien 3 and d) Julien 4

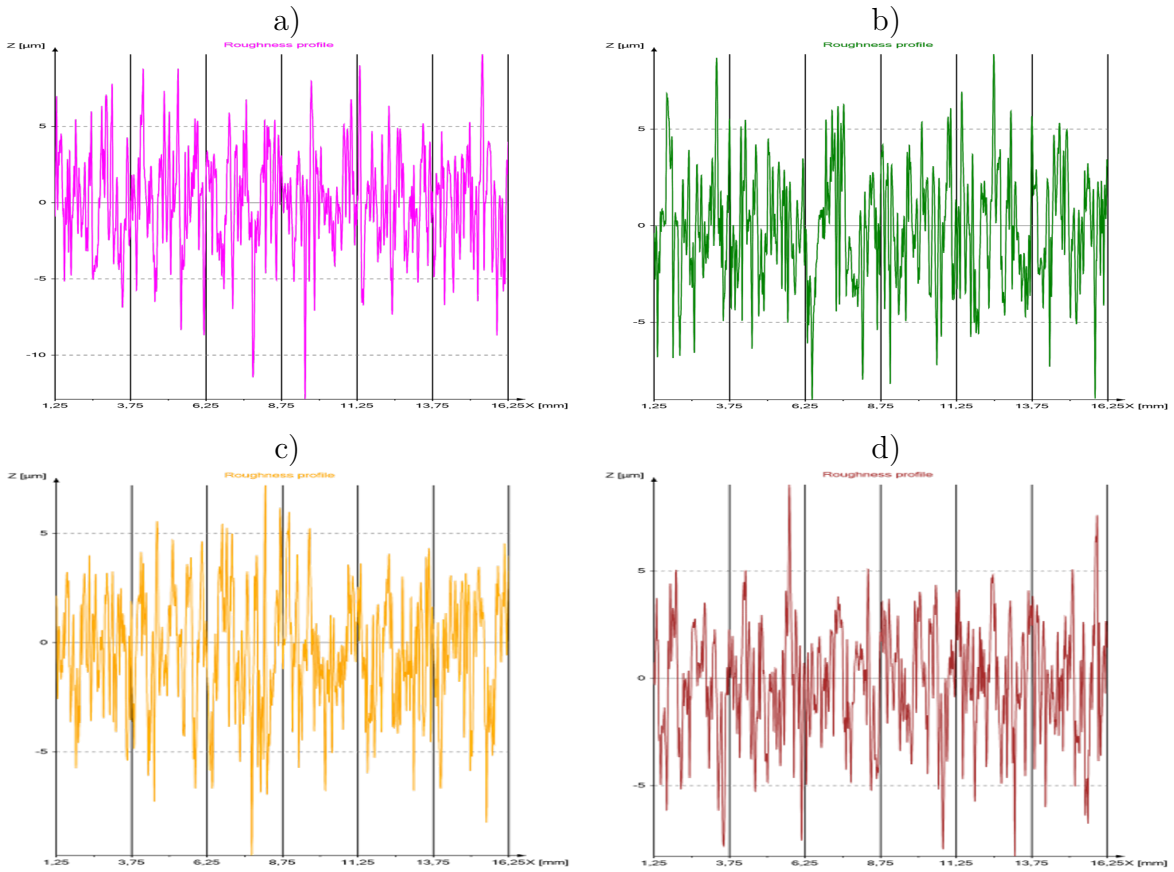

Table A.2: Roughness profile of the rough side of non-treated plates.

Sample	**Ra (μm)**	**Rdc (μm)**	**RSm (mm)**	**RPc (/cm)**
Julien 1	2.49	15.491	0.2102	50
Julien 2	2.28	13.253	0.2558	41
Julien 3	2.12	11.713	0.2451	45
Julien 4	2.02	11.721	0.2546	41

Table A.3: Roughness profile of the smooth side of non-treated plates.

Sample	**Ra (μm)**	**Rdc (μm)**	**RSm (mm)**	**RPc (/cm)**
Julien 1	0.37	2.394	0.2813	13
Julien 2	0.3	2.663	0.3419	7
Julien 3	-	-	-	-
Julien 4	0.37	2.394	0.2813	13

Table A.4: Roughness profile of the non-treated tubes.

Sample	**Ra (μm)**	**Rdc (μm)**	**RSm (mm)**	**RPc (/cm)**
Julien 1	2.57	22.797	0.4969	21
Julien 2	1.96	16.538	0.3792	27
Julien 3	2.00	16.077	0.5948	16
Julien 4	1.98	11.709	0.4221	23

A.2 Contact Angle Measurements

Table A.5: Contact angle images of non-treated and plasma treated Julien 1 and Julien 4 with liquid containing water/ethanol 30/70 wt% at 20° C.

Material	Non-treated	Plasma treated
Julien 1	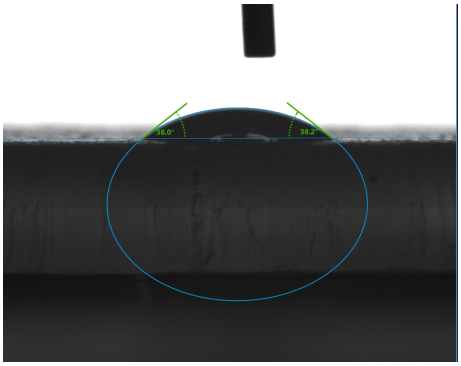	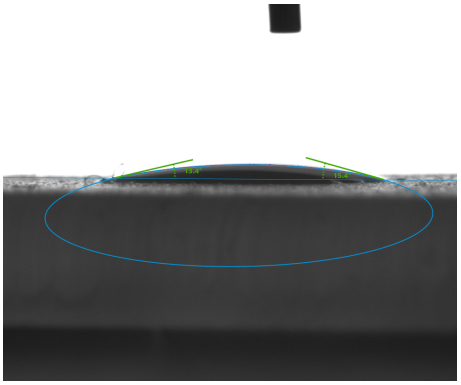
Julien 4	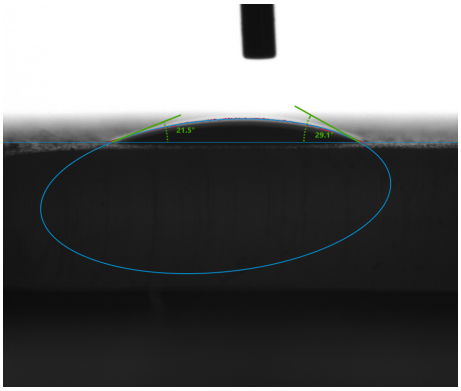	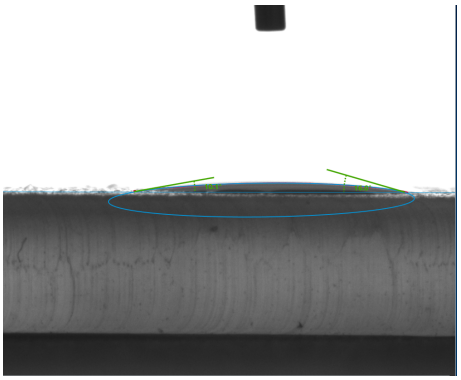

Table A.6: Contact angle measurements for Julien 1-4 with 100 wt% water 20 °.

Material	Contact angle (°)	StDev
Julien 1	95.05	0.05
Julien 2	28.46	5.41
Julien 3	26.59	1.26
Julien 4	27.3	1.6

DEPARTMENT OF CHEMISTRY AND CHEMICAL ENGINEERING
CHALMERS UNIVERSITY OF TECHNOLOGY
Gothenburg, Sweden
www.chalmers.se

CHALMERS
UNIVERSITY OF TECHNOLOGY